MR No. L5C29a

NATIONAL ADVISORY COMMITTEE FOR AERONAUTICS

WARTIME REPORT

ORIGINALLY ISSUED

April 1945 as
Memorandum Report L5C29a

FULL-SCALE-TUNNEL PERFORMANCE TESTS OF THE PV-2 HELICOPTER ROTOR

By Eugene Migotsky

Langley Memorial Aeronautical Laboratory
Langley Field, Va.

NACA

WASHINGTON

MR No. L5C29a

NATIONAL ADVISORY COMMITTEE FOR AERONAUTICS

MEMORANDUM REPORT

for the

Bureau of Aeronautics, Navy Department

FULL-SCALE-TUNNEL PERFORMANCE TESTS OF THE PV-2 HELICOPTER ROTOR

By Eugene Migotsky

SUMMARY

An investigation has been conducted at the Langley full-scale tunnel to obtain basic performance data for the PV-2 helicopter rotor. Blade motion as well as rotor forces and power were measured for the static-thrust condition and for a limited range of forward-flight conditions. Only the force-test data are presented in this paper.

The static-thrust data are presented as the variation of thrust coefficient with torque coefficient. The forward-flight performance data have been reduced to lift coefficients and drag-lift ratios, and the variation of these parameters with pitch angle and tip-speed ratio are given for a series of spindle-angle settings. In addition, charts of convenient form are prepared from which the performance of a helicopter equipped with such a rotor may be obtained rapidly for the range of conditions covered.

The rotor performance is compared with that predicted from theoretical studies and the comparison shows that available theories provide reasonably accurate predictions of helicopter performance if the actual blade-section characteristics are used in the calculations. More detailed analysis of the validity of the theories, especially with regard to second-order effects, is not justified at present because the data available are too limited and tunnel effects are not yet completely evaluated.

INTRODUCTION

Tests have been conducted at the Langley full-scale tunnel to determine the performance characteristics of the PV-2 helicopter rotor. These tests were requested by the Bureau of Aeronautics, Navy Department, and were intended to provide basic performance data on a full-scale helicopter rotor which would be used to determine the validity of existing theory and which would aid in making rational evaluations of proposed helicopter designs.

The tests included photographic observations of the blade motion as well as measurements of the rotor forces and power input to the rotor. These measurements were made for the static-thrust case and over a range of forward-flight conditions. The tip-speed ratio range for the tests in the forward-flight conditions was approximately 0.11 to 0.23. Due to vibrational difficulties it was necessary to conduct the tests at reduced rotor speeds and the tests were, in effect, about two-thirds of full scale.

The reading and computing of the photographic blade-motion records have not been completed except for those readings necessary for the determination of the mean pitch angle at the 0.75 radius. Accordingly, only the results of the force tests are presented. The results of the static-thrust measurements, in coefficient form, have been compared with the analysis of reference 1. The forward-flight performance data have also been reduced to fundamental nondimensional parameters and the variation of these parameters with tip-speed ratio, pitch angle, and spindle-angle setting are given. Since these data cover ranges of helicopter design conditions, a procedure is outlined for applying these results to rotors operating at given flight conditions. The rotor performance for several flight conditions is obtained and these results are compared with the performance predicted by the charts of reference 2.

SYMBOLS

R	rotor-blade radius
b	number of blades

c blade chord of untapered portion

σ rotor solidity, $bc/\pi R$

$\theta_{0.75}$ mean pitch angle at 0.75R

Ω angular velocity, radians per second

α_s spindle-angle setting, positive for rearward spindle tilt

V forward velocity

ρ air density, slugs per cubic foot

μ tip-speed ratio, $V/\Omega R$

T rotor thrust

C_T thrust coefficient, $\dfrac{T}{\rho(\Omega R)^2\pi R^2}$

Q rotor torque

C_Q torque coefficient, $\dfrac{Q/R}{\rho(\Omega R)^2\pi R^2}$

L rotor lift

C_L lift coefficient, $\dfrac{L}{\frac{1}{2}\rho V^2\pi R^2}$

P drag equivalent of shaft power input, $Q\Omega/V$

P/L power drag-lift ratio

$(D/L)_i$ induced drag-lift ratio

$(D/L)_o$ profile drag-lift ratio

$(D/L)_p$ parasite drag-lift ratio

$(D/L)_c$ drag lift ratio representing angle of climb

$(D/L)_r$ rotor drag-lift ratio, $(D/L)_i + (D/L)_o$

$(D/L)_{useful}$ ratio of rotor thrust along flight path to rotor lift

f equivalent flat-plate drag area, $\frac{\text{Parasite drag}}{\frac{1}{2}\rho V^2}$

α_o section angle of attack, measured from zero-lift angle

c_{d_o} section drag coefficient

c_l section lift coefficient

a slope of lift coefficient against section angle of attack (radian measure)

APPARATUS AND TESTS

The PV-2 rotor tested was designed to operate at 371 rpm on a helicopter of 1000 pounds gross weight. The rotor was 25 feet in diameter and had three blades of NACA 0012.6 section (symmetrical section with a maximum thickness ratio of 12.6 percent). The blades were not twisted or tapered, except for cut-outs at the inboard end. Pertinent dimensions of the rotor blades are given in figure 1. The blades had a tubular steel spar, located slightly ahead of the 1/4-chord line, to which wooden ribs were attached. The rib spacing varied between 4 and 8 inches. The forward portion of the blade (approximately 30 to 35 percent of the chord) was covered with plywood and the trailing edge (approximately 10 percent of the chord) was solid wood. This framework was covered with fabric, doped, and polished to a smooth finish. However, irregularities in the contour were apparent.

The rotor was of the articulated type, having hinges that permitted the blades to oscillate in the plane of rotation as well as normal to the plane of rotation. In this rotor design hydraulic dampers were used to absorb the energy of the blade oscillations in the plane of rotation. In addition to these dampers, rubber restrainers were used to restrict elastically the blade flapping and dragging motions. These restrainers were adjusted to exert no force on the blades in normal hovering flight and were relatively soft. For example, when a blade was at its maximum

design flapping angle, the bending moment imposed on the spar by the restrainer was equal to the static weight moment of the blade. Consequently, it is believed that these restrainers would not affect the rotor performance to a measurable degree, especially since the tests were made under trim conditions and the blade motions were relatively small. The pitch angle of the blades was varied by means of a movable-bearing mechanism; moving the bearing parallel to the axis of rotation changed the mean pitch angle of the blades, and tilting the bearing with respect to the axis of rotation provided cyclic variations of pitch angle with azimuth angle.

The rotor was mounted in the jet of the Langley full-scale tunnel with the rotor hub about 20 feet from the entrance cone and approximately on the center line of the jet (fig. 2). Photographs of the setup are shown in figures 3 and 4.

The general assembly of the support system is shown schematically in figure 5. The main support member is a standard 12-inch structural steel pipe, to the base of which were welded a base plate and gusset plates. This column was mounted on a pair of removable support frames which were bolted to the floating frame of the wind-tunnel balance system. The rotor pylon was attached to the top of this column at three support points. In order to permit the spindle angle to be varied, the two front supports were set in trunnions, and the rear support was attached to a jack-screw type of mechanism.

An electric motor was used to drive the rotor. The power input to the rotor was measured by a reaction-type strain-gage torquemeter which was attached to the upper end of the motor casing. The rotor speed was measured by means of a standard aircraft tachometer.

Since the tare drag of the pylon and its supporting structure would be large relative to the rotor drag forces, the entire supporting structure was shielded from the air stream by a fairing. During the tests, this fairing was never in contact with any structure that was connected to the wind-tunnel balances.

All tests were conducted under conditions corresponding to trim about a representative center-of-gravity location, which in this case was taken to be on the axis of rotation and $47\frac{5}{8}$ inches below the center line of the

flapping hinge. Testing under these conditions would not have been practical with the regular wind-tunnel balances since it would require that the controls be adjusted continuously until the readings on five scales fulfilled the desired moment equations. An auxiliary strain-gage balance system was therefore used which gave direct indication of the rotor thrust and the pitching and rolling moments. The lift and drag data presented, however, were obtained from the wind-tunnel balances.

In order to determine the oscillations and deflections of the blades, grain-of-wheat bulbs were installed at three radial locations on the leading and trailing edges of one of the blades. A 35-millimeter motion-picture camera mounted on the rotor hub and rotating with it recorded the various blade motions. The mean pitch angle at the 0.75 radius station was determined from these camera records by plotting the pitch-angle variation with azimuth angle and finding the average value.

Before the rotor tests were made, vibration surveys (with a shaker in place of the rotor) were conducted to determine the vibrational characteristics of the wind-tunnel setup. It was found that the flexibility of the supporting structure was sufficient to make its natural frequency too low for safe operation. The support structure was then reinforced and several flying wires were used to guy the main support column. These modifications raised the natural frequency enough to permit testing up to rotor speeds of about 300 rpm, which was still below the design rotor speed (371 rpm). Testing at these lower rotor speeds, in effect, corresponded to testing at less than full scale.

The static-thrust tests were made with the spindle angle set vertically and the tunnel off. At several rotor speeds the thrust and torque were measured for the entire range of pitch angles (about 2° to 9°).

For the forward-flight tests the rotor lift, drag, and torque were measured at several rotor speeds, tip-speed ratios, and spindle-angle settings. It should be noted that the minimum tip-speed ratio obtainable with a given rotor in the Langley full-scale tunnel is limited since the lowest steady air stream velocity is about 30 miles per hour. The corresponding minimum value

of tip-speed ratio was about 0.11 for the rotor speeds attainable in these tests.

With the blades removed from the rotor hub, tests were made to determine the lift, drag, and torque tares of the camera installation and that part of the rotor hub exposed to the air stream. These tares, which do not include the drag of the blade shanks, were subtracted from the rotor test data, and the results presented thus represent the characteristics of the rotor blades alone.

The tare data obtained with zero airspeed as well as with the tunnel operating showed that the readings of the wind-tunnel balances became irregular and unreasonable as soon as the rotational speed exceeded approximately 280 rpm. Because of this response of the scales to frequencies in this range, no data for rotational speeds above 280 rpm have been included in this report. The data obtained at the reduced rotor speeds correspond, in effect, to those of a rotor tested at about two-thirds of full scale.

The data presented for the forward-flight conditions have been corrected for jet-boundary effects by assuming that the rotor acts essentially as an airfoil of equal lift and span.

RESULTS AND DISCUSSION

Static Thrust

The results of the static-thrust measurements are presented in figure 6 as the variation of thrust coefficient with torque coefficient for three rotor speeds. Since no consistent variation with rotor speed was apparent, only one curve was faired through the experimental points.

For comparison with this experimental curve, three theoretical curves were calculated on the basis of the methods given in reference 1. In these methods, the blade-section characteristics are assumed to be of the form

$$c_l = a\alpha_0$$

$$c_{d_0} = \delta + \epsilon\alpha_0^2$$

In computing the variation of thrust and torque coefficients by this method the constants in the equations were chosen to give an approximation to the section characteristics obtained from unpublished wind-tunnel tests of a similarly constructed blade; these values were

$$a = 5.56 \text{ per radian}$$

$$\delta = 0.0084$$

$$\epsilon = 0.400$$

A comparison of the section characteristics corresponding to these values with the unpublished data mentioned above is shown in figure 7. The upper curve of figure 6 was calculated using these constants.

In order to obtain agreement with the results of model rotor tests it was necessary, in reference 1, to introduce certain empirical corrections in the calculations of the torque and thrust coefficients. The correction for the torque coefficients involved the use of a correlation factor K, the value of which was found to be 1.67, and the drag equation effectively became

$$c_{d_o} = \delta + K\epsilon a_o^2$$

$$= \delta + 1.67\epsilon a_o^2$$

The curve of figure 6 indicated as "theory with empirical torque correction (K = 1.67)" was calculated on this basis.

For the thrust coefficient, where an appreciable difference existed between the theoretical and the experimental results, no attempt was made in reference 1 to modify the theoretical equations, and the empirical relations were proposed as generally applicable. The curve of figure 6 indicated as "theory with empirical torque and thrust corrections" was obtained by correcting the theoretical thrust by the same difference that was found in reference 1 between the theoretical and experimental thrust values. The torque coefficient for this curve was found as for the preceding curve.

Inspection of the four curves of figure 6 shows that using the correlation factor K improves the agreement with the data but that the theory is still slightly optimistic. The empirical thrust correction appears to be of the correct magnitude at the higher thrust coefficients covered in these tests but seems too large at the lower thrust coefficients. A more detailed comparison of the theory with these results is not justified because of the unknown effects of the flow around the test chamber and of the proximity of the balance-house roof. It is believed, however, that these effects are relatively small in this case and that the analysis of reference 1 offers a reasonably accurate prediction of the fundamental performance characteristics of a helicopter rotor in the static-thrust condition.

Forward Flight

The performance data obtained for the forward-flight conditions have been reduced to lift coefficients and drag-lift ratios; and the variations of these parameters with pitch angle, tip-speed ratio, and spindle-angle setting are presented. In general, the discussion of rotor losses and shaft-power input in terms of drag-lift ratios follows along the same lines as in reference 2, through the equation

$$\frac{P}{L} = \left(\frac{D}{L}\right)_i + \left(\frac{D}{L}\right)_o + \left(\frac{D}{L}\right)_p + \left(\frac{D}{L}\right)_c \qquad (1)$$

In this equation, P represents the drag equivalent of the shaft-power input:

$$P = \frac{\text{Shaft-power input}}{\text{Velocity}}$$

$$= \frac{Q\Omega}{V}$$

and the D's similarly represent the drag equivalent of the power required to overcome the induced and profile drag of the blades, to overcome the parasite drag of the fuselage, and to maintain a steady climb.

In presenting and applying the results of wind-tunnel tests of an isolated helicopter rotor it is convenient to use a modified form of equation (1) in which the drag-lift ratios on the right-hand side are combined to give

$$\frac{P}{L} = \left(\frac{D}{L}\right)_r + \left(\frac{D}{L}\right)_{useful} \qquad (2)$$

where $(D/L)_r$ now corresponds to the total rotor losses (induced + profile), and $(D/L)_{useful}$ becomes the ratio of the thrust along the flight path to the rotor lift.

From the measurements taken during the wind-tunnel tests it was possible to calculate directly the quantities P/L (from the power, the tunnel airspeed, and the lift measured on the balances) and $(D/L)_{useful}$ (from the drag and lift forces measured on the balances). From these parameters the rotor losses $(D/L)_r$ were computed by the relationship given in equation (2).

The parameters C_L, P/L, and $(D/L)_r$ were first plotted against pitch angle at the 0.75 radius for different tip-speed ratios at fixed spindle-angle settings. Figures 8(a) to 8(c) show these variables plotted in this manner for the spindle-angle setting of -5.5°, and are presented primarily to indicate the order of magnitude of the scatter in the data. It should be noted that the fixed spindle-angle setting does not correspond to a fixed aerodynamic angle of attack of the rotor disk since the effect of the jet boundaries on the direction of the air stream is a function of the rotor lift coefficient, and hence is not constant for these figures. The correction to the spindle-angle setting is given in figure 9 as a function of lift coefficient. Furthermore, if the behaviors of different rotors are to be compared on the basis of angle of attack, the angle of attack of the spindle axis is of no great importance without knowledge of the blade flapping or cyclic pitch variation. Since the blade-motion data are not available at present, it was found expedient to use the uncorrected spindle-angle setting as a parameter for the presentation of the performance data. A method is outlined later in the discussion by which the force data can be applied, without having the aerodynamic angle of attack of the rotor, to obtain the performance of a helicopter operating with the PV-2 rotor under various design conditions.

From the original plots of C_L, P/L, and $(D/L)_r$ against $\theta_{0.75}$, cross plots were made to obtain the variation of these parameters with tip-speed ratio for constant values of pitch angle and spindle-angle setting. These cross plots are presented in figures 10 to 12. It will be noticed that the data were not obtained over identical ranges of pitch angle and tip-speed ratio. It was necessary to limit the range of test conditions at the higher pitch angles and tip-speed ratios because of the vibrations encountered at these conditions.

It is evident that the data as presented do not correspond directly to the flight conditions of the rotor operating on a particular helicopter design but cover a range of design conditions. A method is therefore outlined to indicate how these data can be applied to determine the performance of a helicopter (with a rotor similar in design to the rotor tested) under a given set of conditions.

It is assumed that the following characteristics of the helicopter are known: gross weight, rotor radius, rotor speed, and parasite drag. It is also assumed that the machine is operating in level flight under standard conditions and that the rotor angle of attack is small so that the lift can be taken to be equal to the thrust.

From these known characteristics the thrust coefficient C_T can be computed. Then, for a desired forward speed, or tip-speed ratio, the lift coefficient is calculated from the relation

$$C_L = \frac{2C_T}{\mu^2}$$

The value of $\theta_{0.75}$ corresponding to these values of C_L and μ is determined from figure 10 for each spindle-angle setting. Having $\theta_{0.75}$ for the desired μ, P/L, and $(D/L)_r$ are obtained from figures 11 and 12, respectively, and $(D/L)_{useful}$ is then calculated from equation (2). These values of $\theta_{0.75}$, P/L, $(D/L)_r$, and $(D/L)_{useful}$ are found for each

spindle-angle setting presented and then plotted against spindle-angle setting. With the variables plotted in this manner it is necessary only to determine the spindle-angle setting which corresponds to the desired level-flight conditions. The procedure is to calculate the ratio $(D/L)_p$ from the given parasite drag and gross weight and then to find, from these plots, the spindle-angle setting for which $(D/L)_{useful}$ equals this value of $(D/L)_p$. This method can be applied to a helicopter in steady climb if, in the determination of α_s, the additional thrust along the flight path required to maintain a steady climb is added to the parasite drag. In order to obtain the variation of the performance parameters with forward velocity, or tip-speed ratio, the foregoing procedure is merely repeated for several values of μ. Following this procedure, the performance characteristics of the rotor operating at thrust coefficients of 0.00268, 0.00364, and 0.00446 were obtained. The thrust coefficient 0.00364 represents the design disk loading of 2.04 for the PV-2 helicopter (25-foot-diameter rotor operating at 371 rpm with a gross weight of 1000 pounds). The other thrust coefficients correspond to disk loadings of 1.50 and 2.50 when the rotor speed and diameter are kept fixed or, when the disk loading is held constant, correspond to rotor speeds of 432 and 335 rpm.

The values of $\theta_{0.75}$, P/L, $(D/L)_r$, and $(D/L)_{useful}$ were found for six values of μ ranging from 0.12 to 0.22 at each spindle-angle setting. In view of the scatter in the data and the limited number of spindle-angle settings at which these data were available, straight lines were faired through the values obtained. These results are presented in the charts of figure 13. With these charts it is necessary to determine only the lift coefficient and $(D/L)_p$ of the helicopter and, by interpolating between the curves, the rotor performance can be estimated directly for the range of conditions represented in the charts.

It can be seen in figure 13 that the variation of $(D/L)_r$ with α_s is relatively small. At the lower tip-speed ratios $(D/L)_r$ decreases slightly with forward tilt of the spindle and, with increasing tip-speed ratio, this effect diminishes until, at the higher tip-speed ratios, there appears to be a tendency

for $(D/L)_r$ to increase with forward spindle tilt. Consequently, since $(D/L)_p$ determines the spindle angle for a given set of operating conditions a relatively large error in estimating this ratio results in second-order errors in estimating the rotor losses.

Since fuselage-drag data are not available for the PV-2 helicopter, it is assumed that an equivalent flat-plate drag area f equal to 7 square feet represents the parasite drag of the machine, and performance estimates were made on this basis. For horizontal flight of this assumed machine, the variation of $\theta_{0.75}$, P/L, and $(D/L)_r$ with tip-speed ratio, for the three values of thrust coefficient chosen, are given in figures 14(a), 14(b), and 14(c). (For $C_T = 0.00446$ these values were obtained by extrapolating the curves of figure 13 to small positive values of α_s.) Also included in these figures are the theoretical variations of these parameters as determined from the charts of reference 2. A comparison of the section characteristics used in reference 2 with those obtained from unpublished wind-tunnel tests of a section of a PV-2 rotor blade is given in figure 15. The difference between the drag curves arises from the fact that the values used in reference 2 were representative of those attainable with blades having a relatively smooth and accurate contour and having an airfoil section with appreciable camber.

In general, there appears to be a discrepancy between the pitch angles predicted by the theory and those measured in the tests, the measurements showing the lower values of pitch angle. This difference is about 1.25° and appears to be approximately constant within the accuracy of the pitch-angle measurements. Analysis of these differences led to the belief that this discrepancy is not due to the inadequacy of the theory but rather to an error made in the reference to which the pitch angle was measured. Such a constant error in pitch-angle measurement, however, does not alter the relationship between the force parameters, and the method outlined for applying the data to specific conditions is still valid.

At the lowest thrust coefficient (0.00268) good agreement exists between the force ratios determined from the test results and the theory. At higher thrust

coefficients the rotor losses predicted from the charts of reference 2 are optimistic and the difference increases with increasing thrust coefficient and decreasing tip-speed ratio. These trends are more apparent in figure 16 where the rotor losses $(D/L)_r$ are plotted against disk loading for three values of tip-speed ratio.

The divergence of the theoretical and experimental curves with increasing thrust coefficient can be attributed, at least in part, to the divergence between the corresponding drag polars as shown in figure 15. The analysis of reference 2 would probably give a more accurate prediction of the performance of this rotor if the actual section drag curve was used or, at least, a better approximation to it.

The larger differences between theory and experiment at the lower tip-speed ratio may be partly due to inaccuracies in the jet-boundary corrections, which are largest at the low tip-speed ratios (that is, at the high lift coefficients). The corrections applied to the D/L ratios shown on figures 13 and 14 varied from a maximum of 0.034 at the highest lift coefficient to a minimum of 0.007 at the lowest lift coefficient. The differences between theory and experiment, however, seem to be too large to be totally ascribable to this effect.

The dependence of the rotor horsepower required on the operating conditions can be seen in figures 17 and 18 in which horsepower-velocity polars are presented for the same value of parasite drag and the same three values of thrust coefficient used in the previous discussion. In the first case (fig. 17) the three values of thrust coefficient were obtained by keeping the rotor tip speed constant and changing the disk loading. Here the power required increases with thrust coefficient, due primarily to the higher downwash velocities in the wake which result in greater induced losses. In the second case (fig. 18) the disk loading was held constant and the different thrust coefficients were obtained by changing the rotor tip speed. Here the power required decreases with increasing thrust coefficient. The saving in power obtained by reducing the rotor speed at constant disk loading results from operating closer to the optimum profile drag-lift ratio of the rotor since the induced losses are essentially the same at each thrust coefficient. As before, the agreement with the theoretically predicted curves is quite close except toward the higher thrust coefficients.

CONCLUDING REMARKS

The performance characteristics of the PV-2 rotor have been determined over a range of conditions. Convenient charts for the forward-flight range covered in these tests have been prepared from which the performance of a helicopter equipped with such a rotor may be predicted. The results of the investigation indicate that the theoretical methods employed in reference 1 (static thrust) and reference 2 (forward flight) will provide reasonably accurate results when the actual blade-section characteristics are used in the computations. A more detailed analysis of the validity of the theories, particularly with regard to second-order effects, is not believed to be justified with the present state of knowledge. In order to obtain a more detailed comparison, blade-motion data as well as force-test data should be available for a wider range of conditions than were covered in these tests. Furthermore, such a comparison would still be somewhat clouded until the effects of the jet boundaries, the proximity of the balance-house roof, and the restraintof the test-chamber walls on the air flow and rotor forces have been determined.

Langley Memorial Aeronautical Laboratory
National Advisory Committee for Aeronautics
Langley Field, Va.,

REFERENCES

1. Knight, Montgomery, and Hefner, Ralph A.: Static Thrust Analysis of the Lifting Airscrew. NACA TN No. 626, 1937.

2. Bailey, F. J., Jr., and Gustafson, F. B.: Charts for Estimation of the Characteristics of a Helicopter Rotor in Forward Flight. I - Profile Drag-Lift Ratio for Untwisted Rectangular Blades. NACA ACR No. L4H07, 1944.

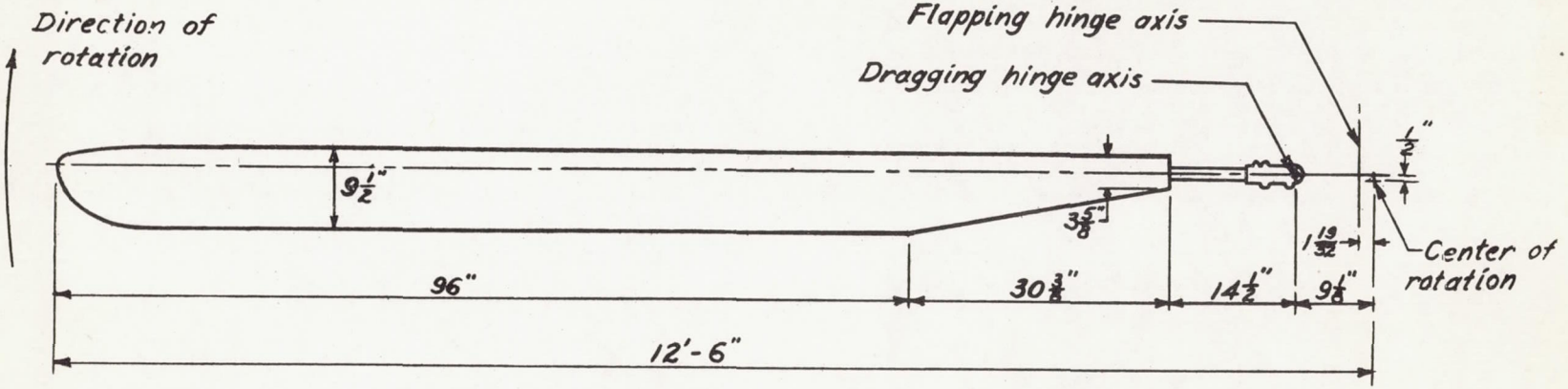

NATIONAL ADVISORY
COMMITTEE FOR AERONAUTICS.

Figure 1.- Dimensions of PV-2 helicopter rotor blade.

MR No. L5C29a

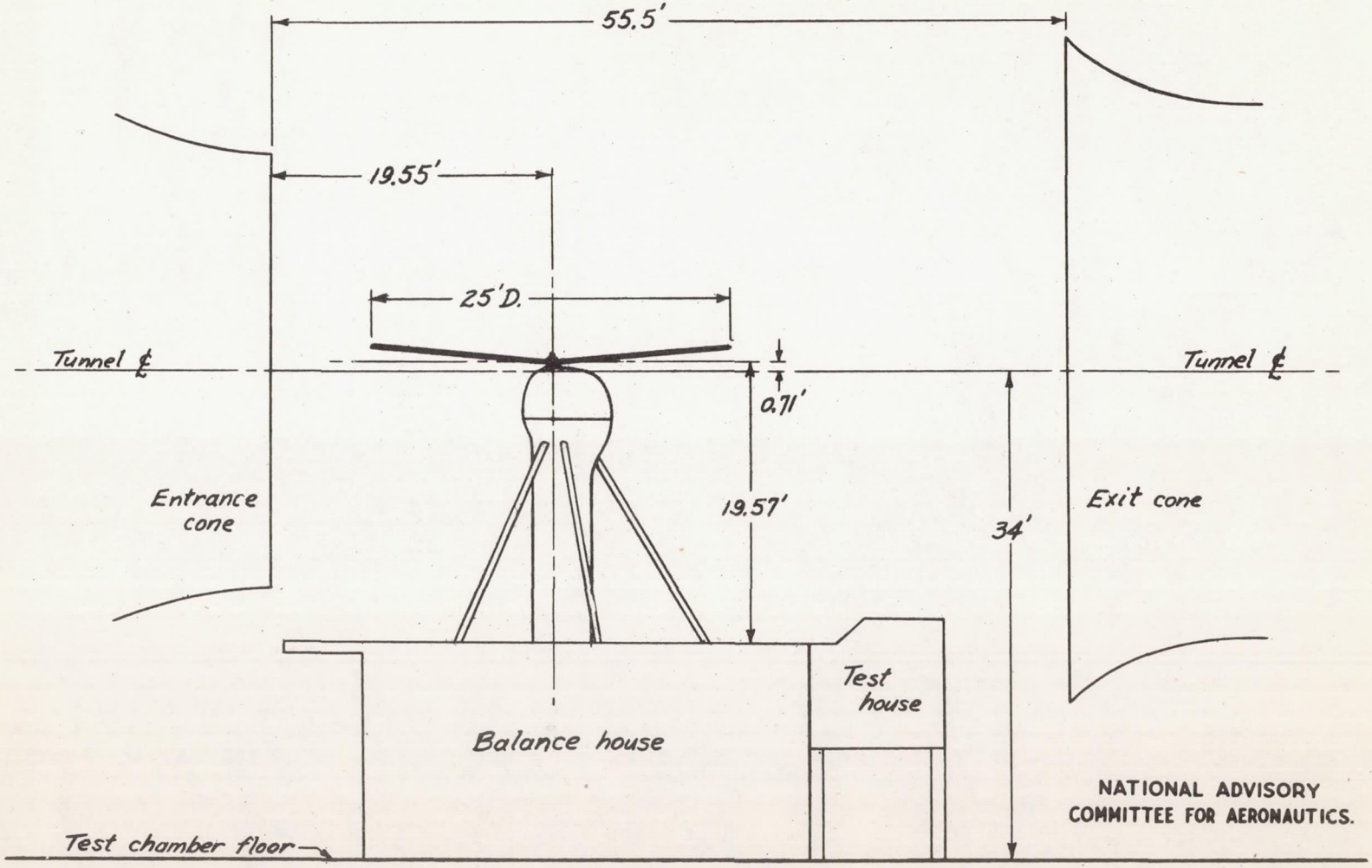

Figure 2.- Location of PV-2 helicopter rotor in the Langley full-scale tunnel.

MR No. L5C29a

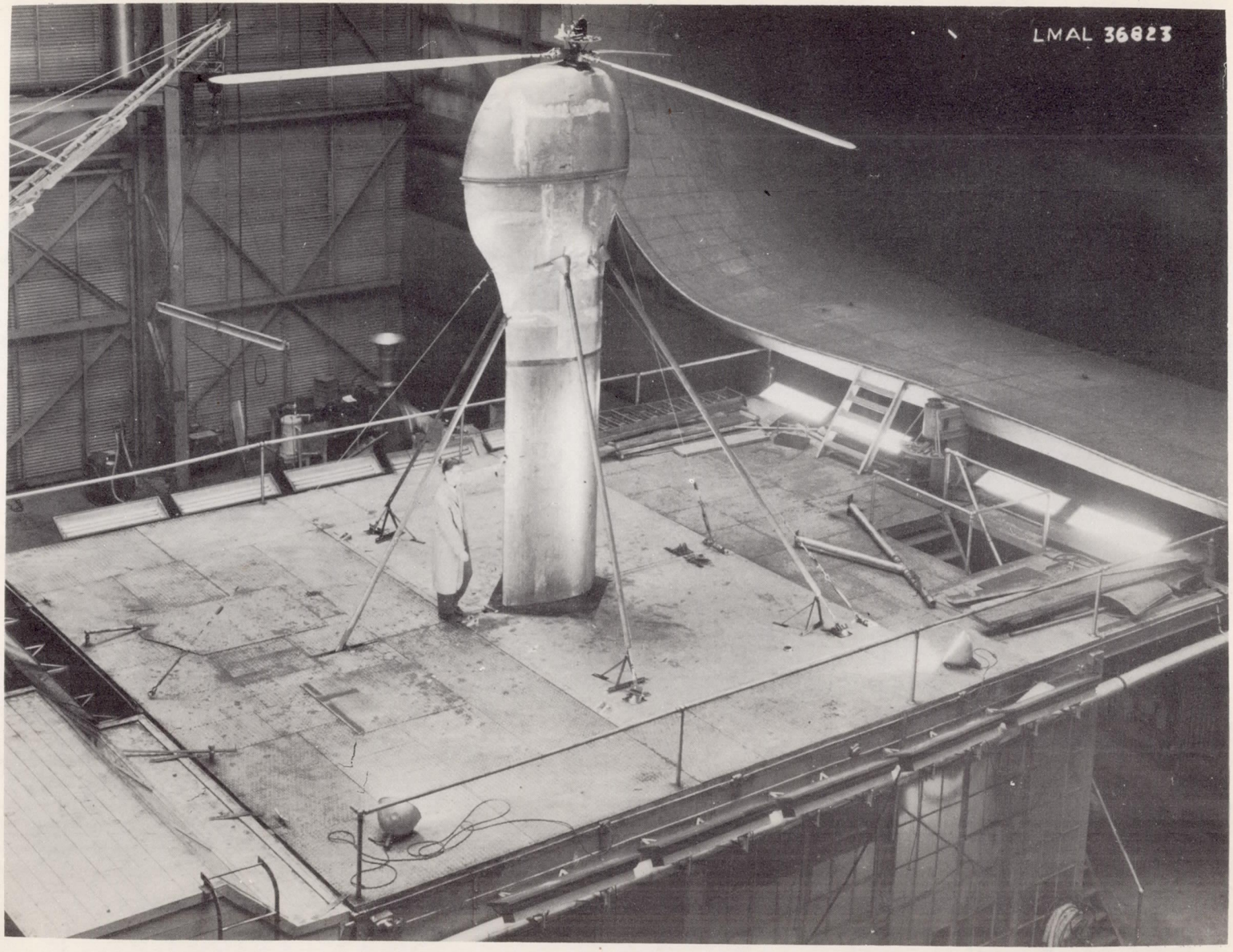

Figure 3.- General view of PV-2 helicopter rotor mounted in the Langley full-scale tunnel.

MR No. L5C29a

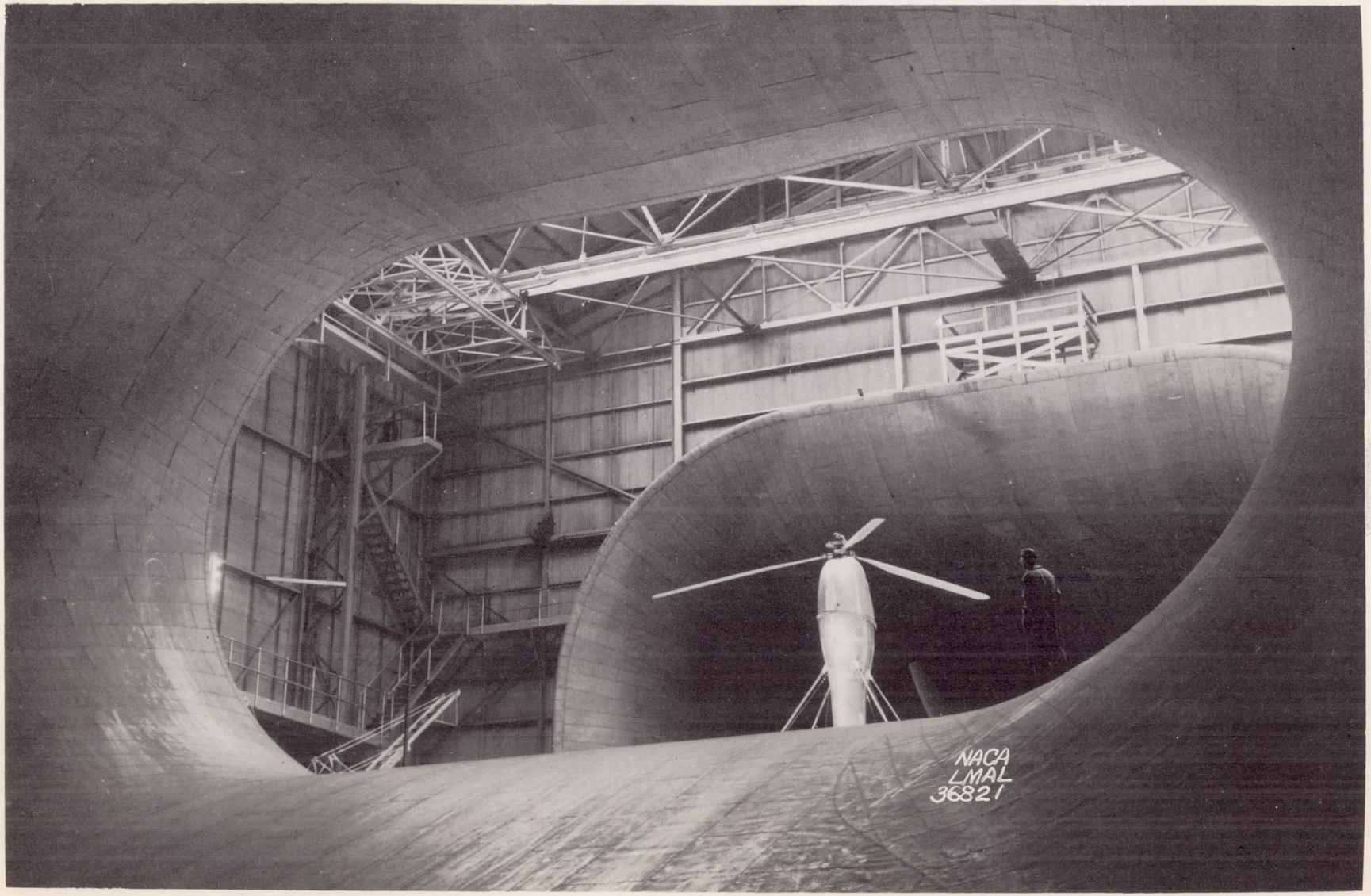

Figure 4.- PV-2 helicopter rotor mounted in the Langley full-scale tunnel as viewed from the entrance cone.

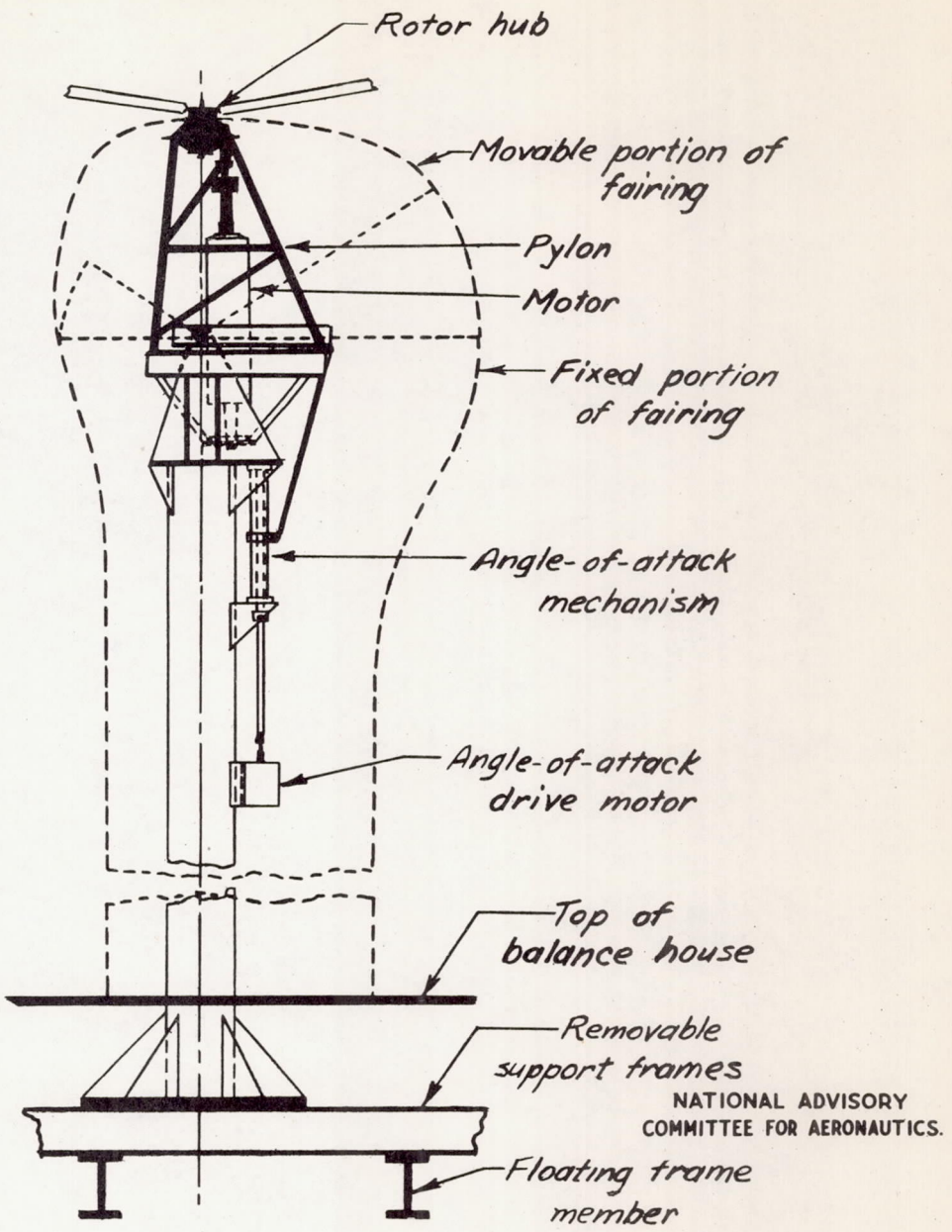

Figure 5.- General assembly of support system for tests of PV-2 helicopter rotor in the Langley full-scale tunnel.

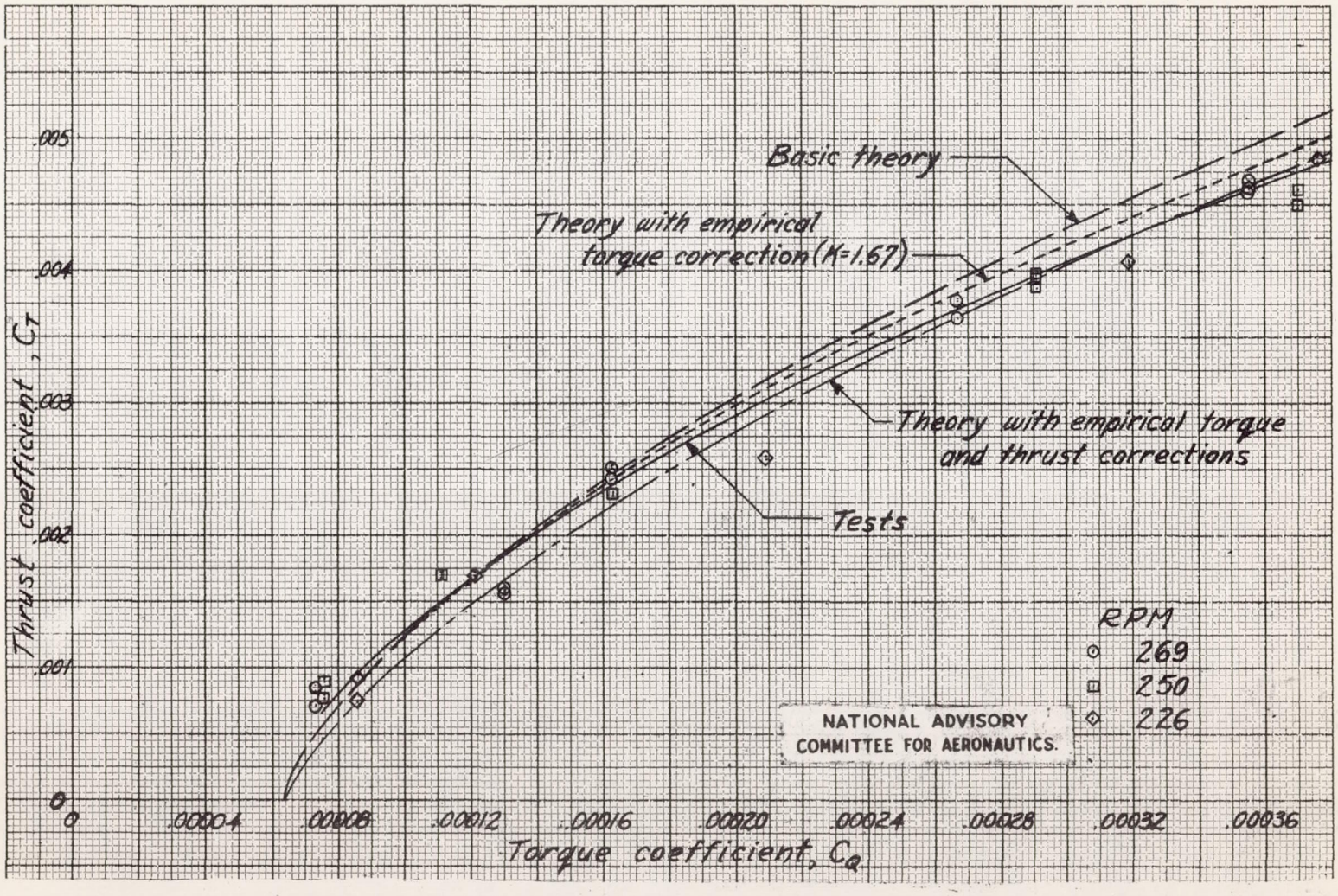

Figure 6.- Variation of thrust and torque coefficients for the PV-2 helicopter rotor in the static-thrust condition. Theoretical curves based on reference 1; $\gamma = 0.0605$; $\delta = 0.0084$; $\epsilon = 0.400$; $a = 5.56$ per radian.

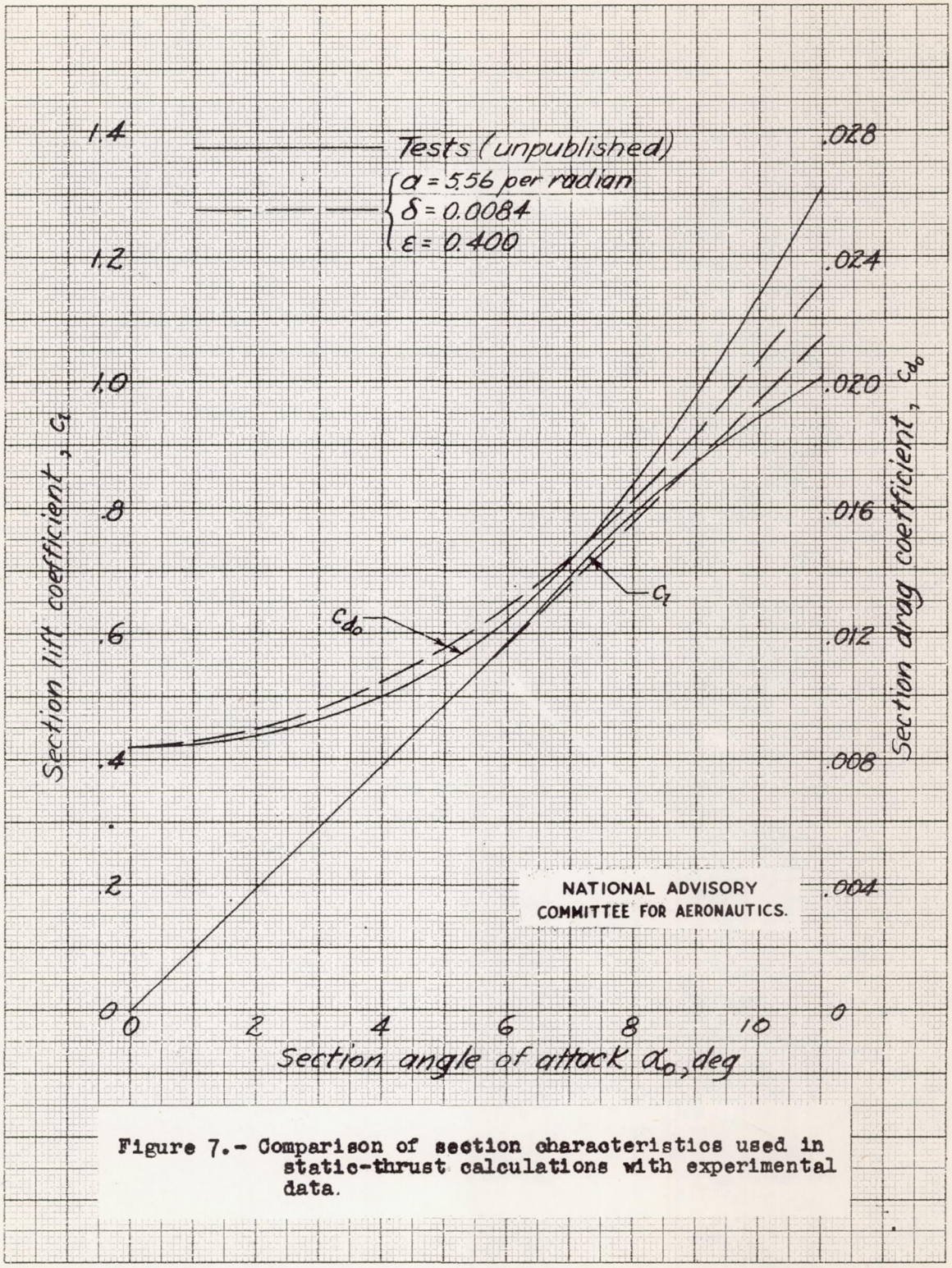

Figure 7.- Comparison of section characteristics used in static-thrust calculations with experimental data.

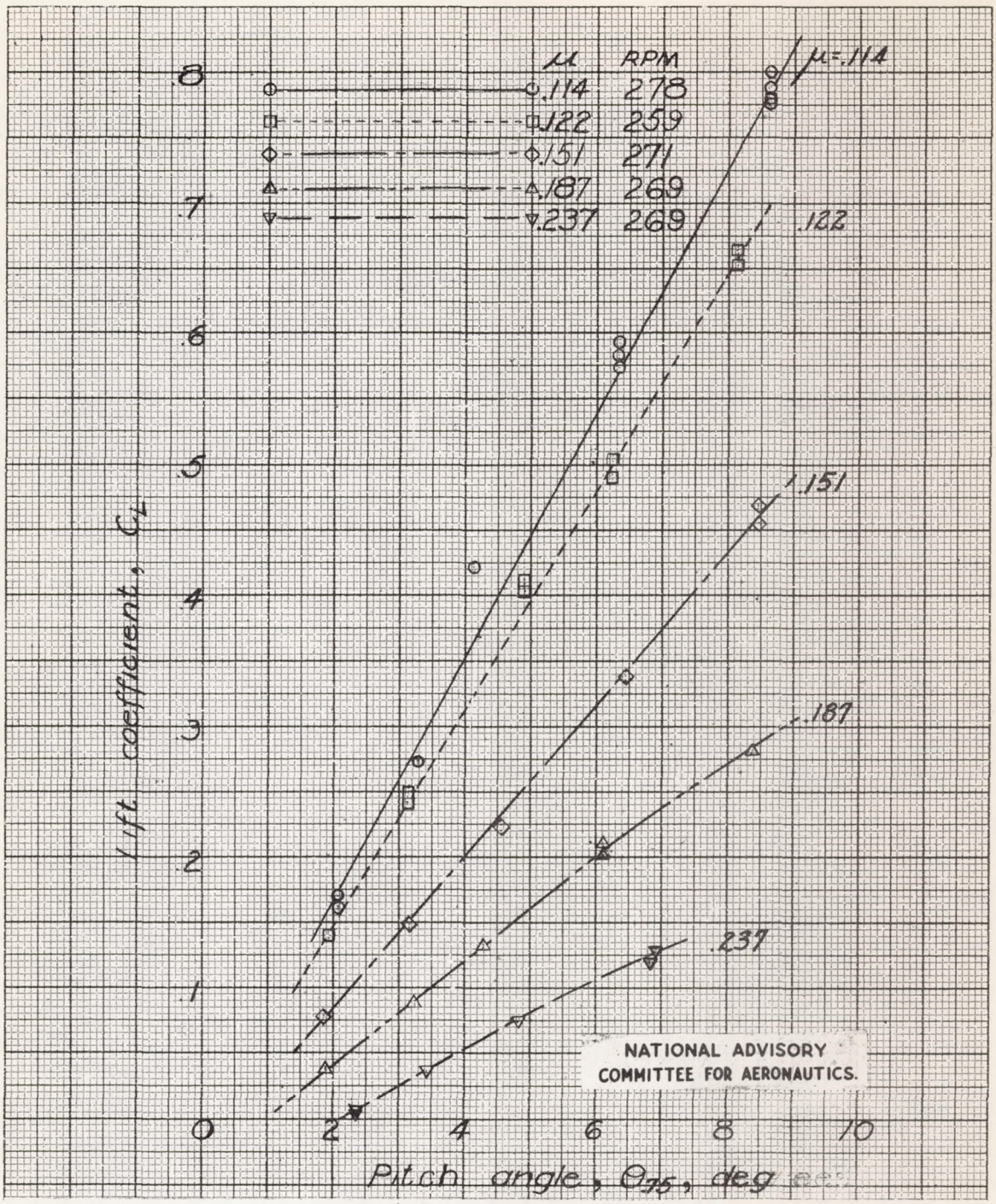

(a) Lift coefficient.

Figure 8.- Variation of aerodynamic characteristics with pitch angle for several values of tip-speed ratio; PV-2 helicopter rotor, $\alpha_s = -5.5°$.

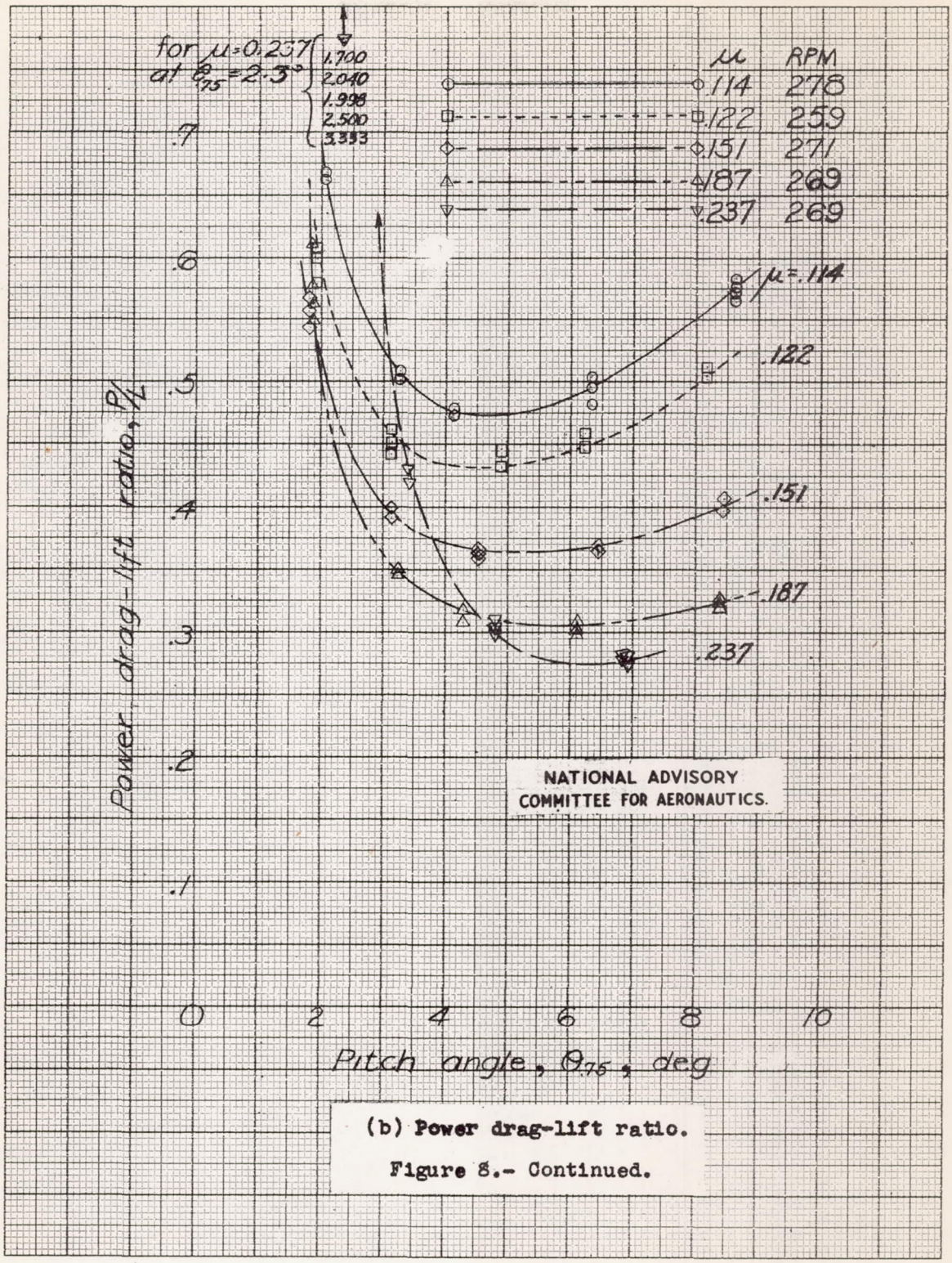

(b) Power drag-lift ratio.

Figure 8.- Continued.

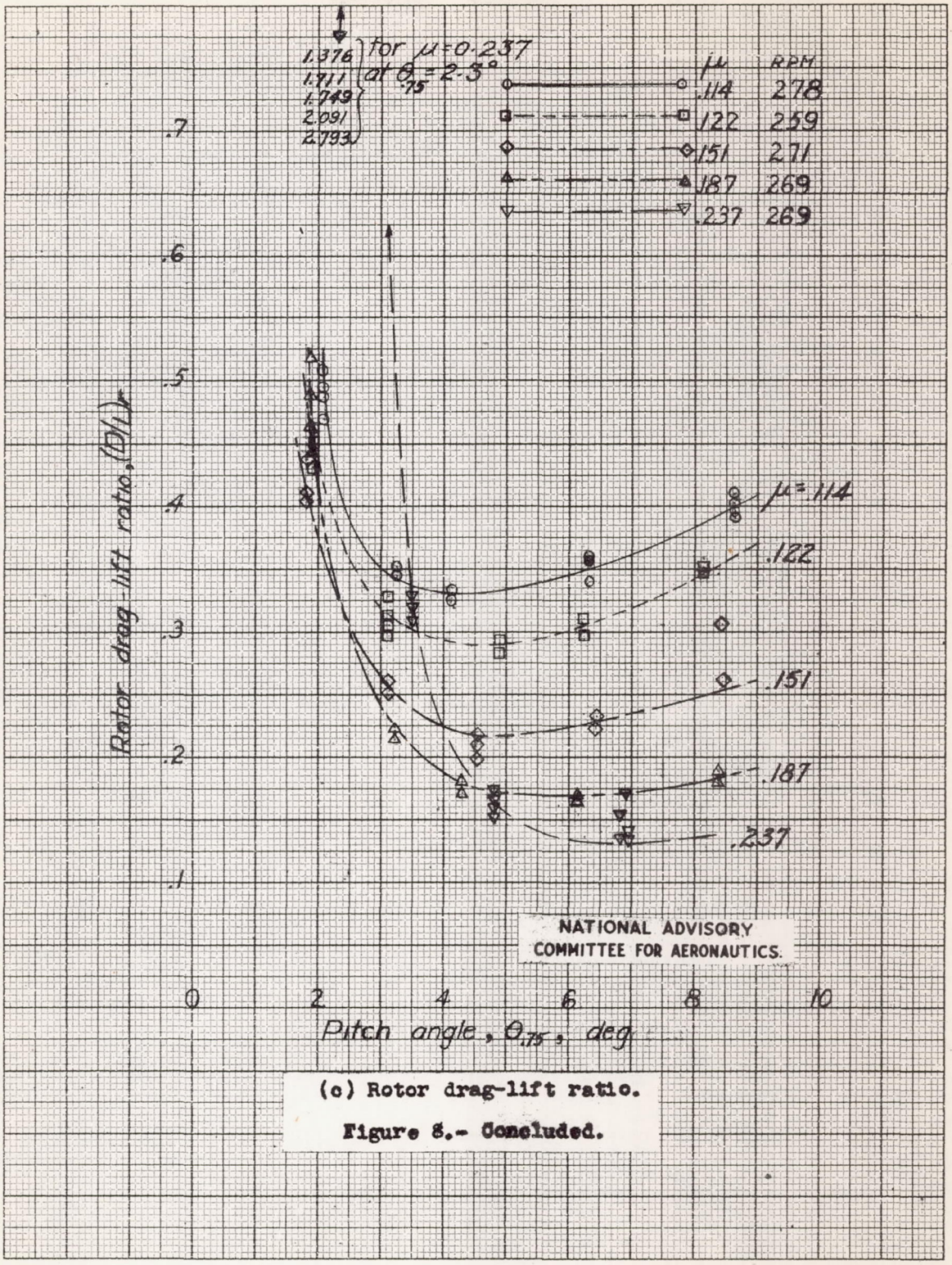

(c) Rotor drag-lift ratio.

Figure 8.- Concluded.

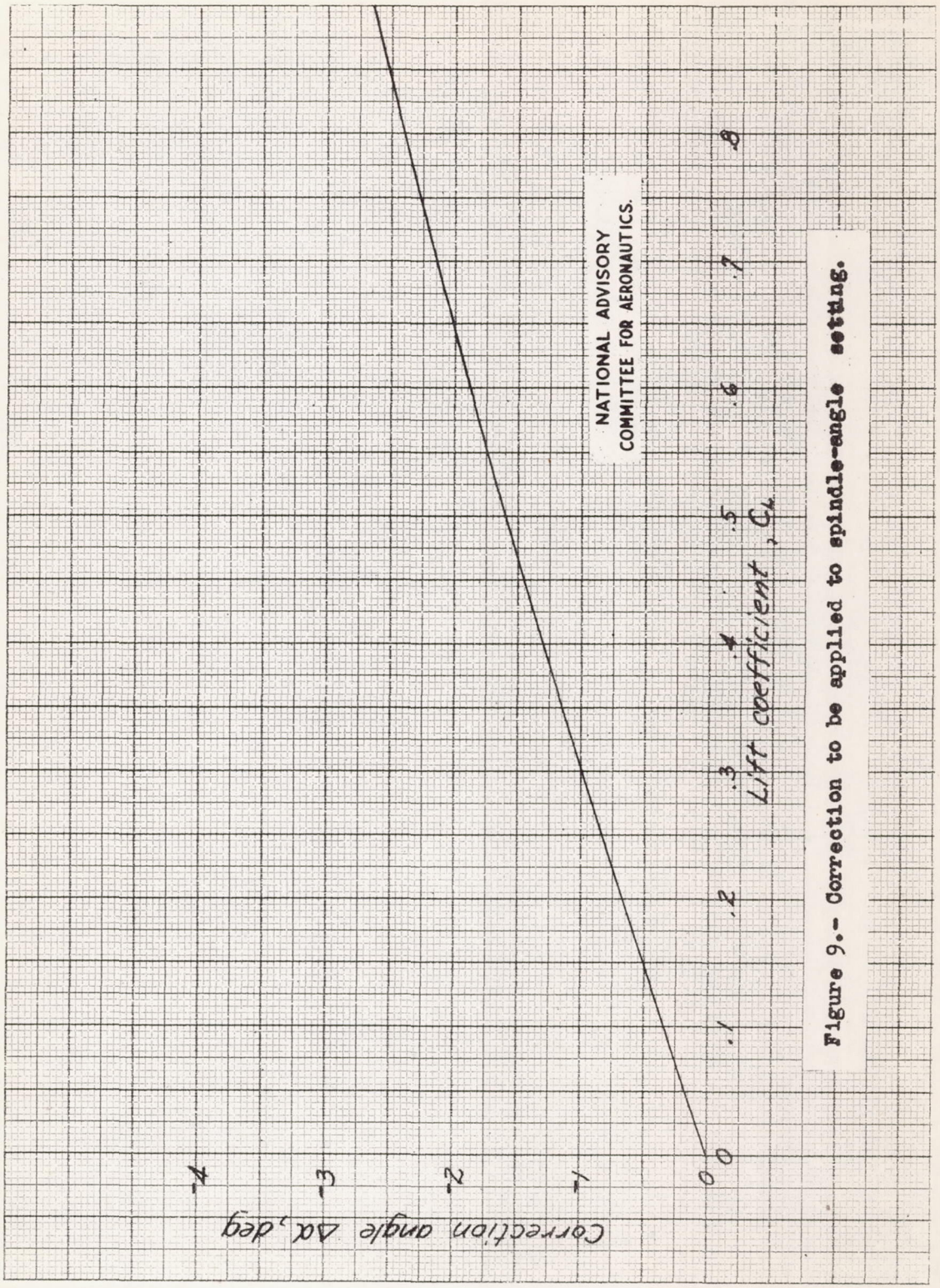

Figure 9.- Correction to be applied to spindle-angle setting.

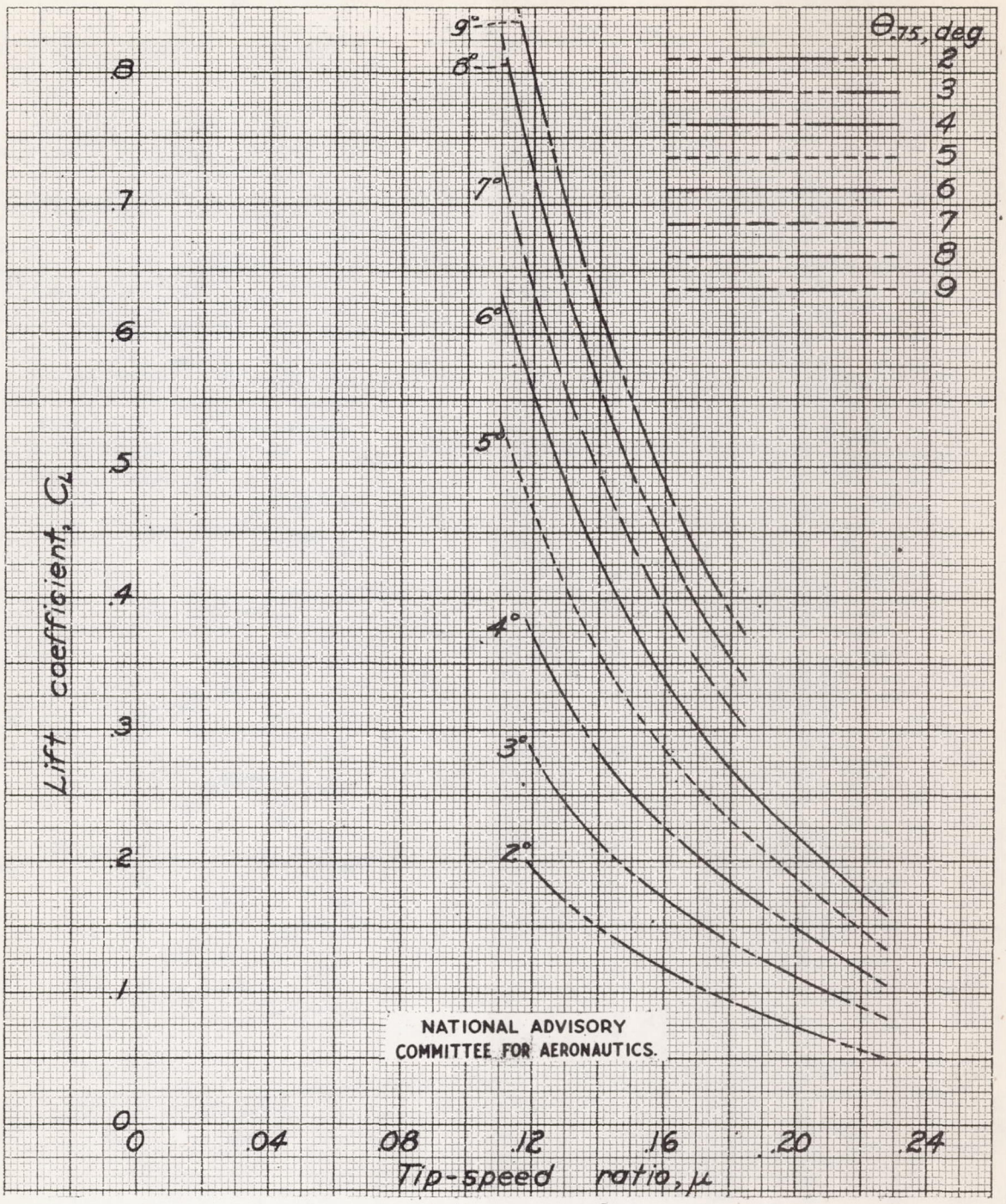

(a) α_s, -0.5°.

Figure 10.- Variation of rotor lift coefficient with tip-speed ratio for different values of pitch angle. PV-2 helicopter rotor; rotor speed, approximately 270 rpm.

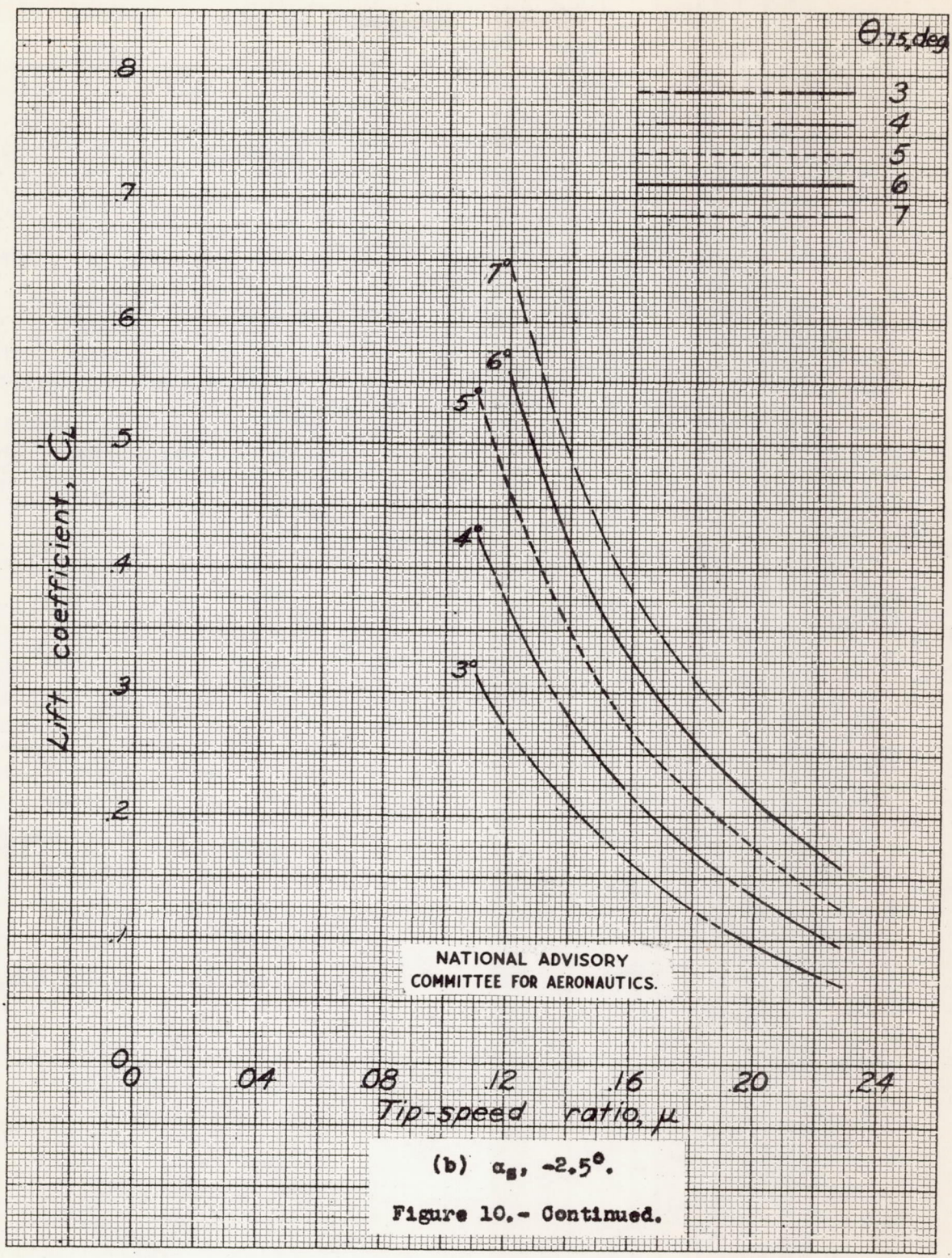

(b) α_s, -2.5°.

Figure 10.- Continued.

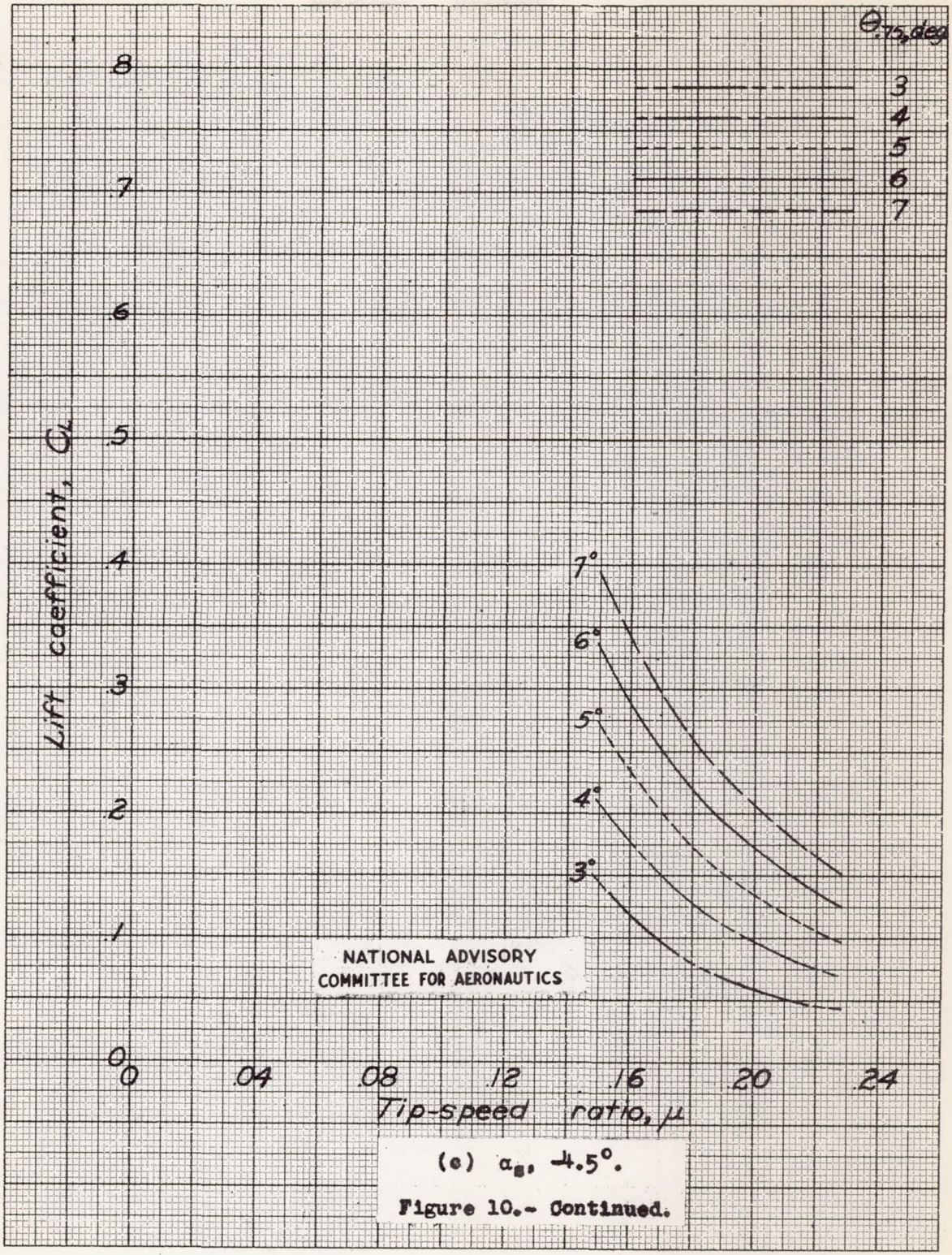

(c) α_s, -4.5°.

Figure 10.- Continued.

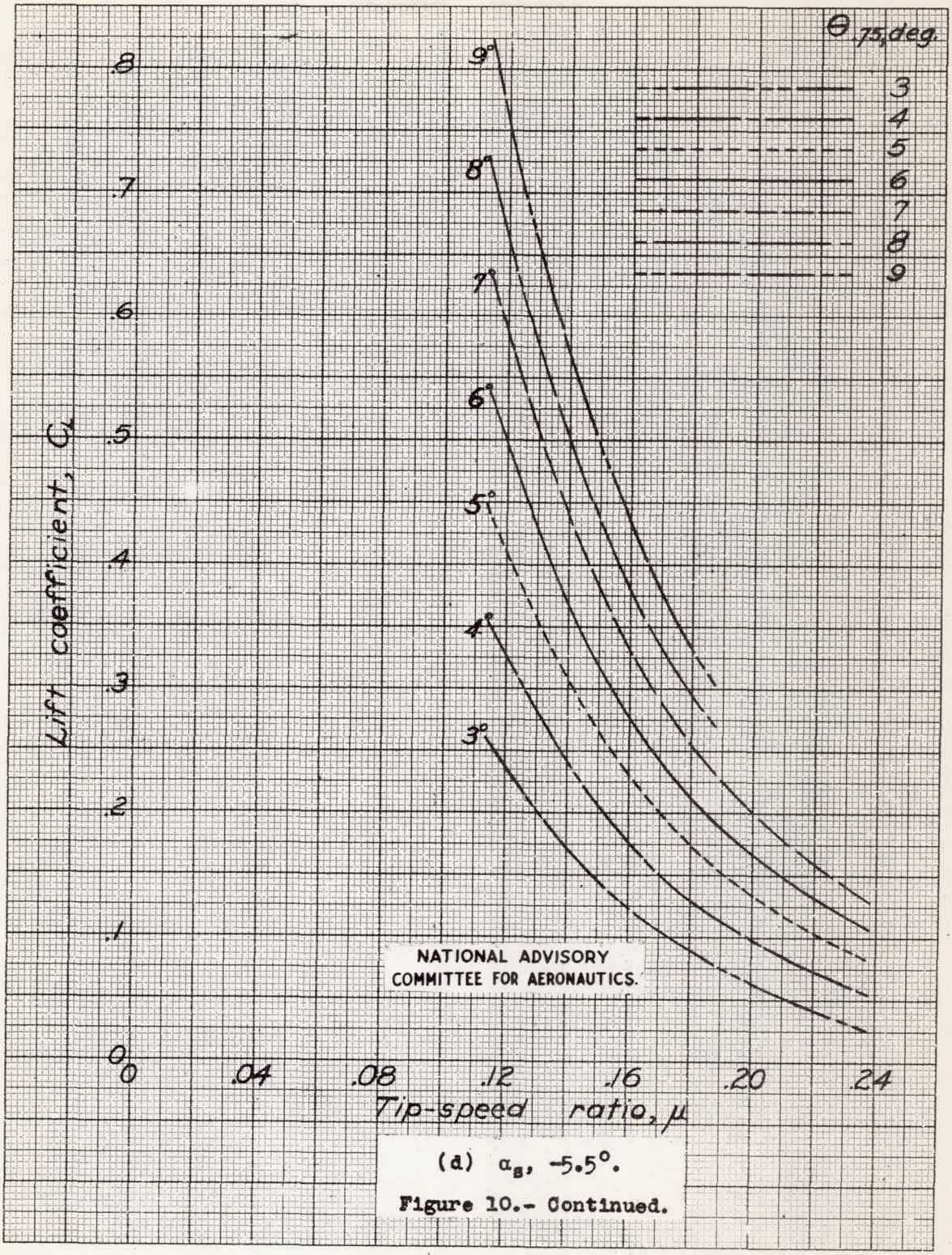

(d) α_s, -5.5°.

Figure 10.- Continued.

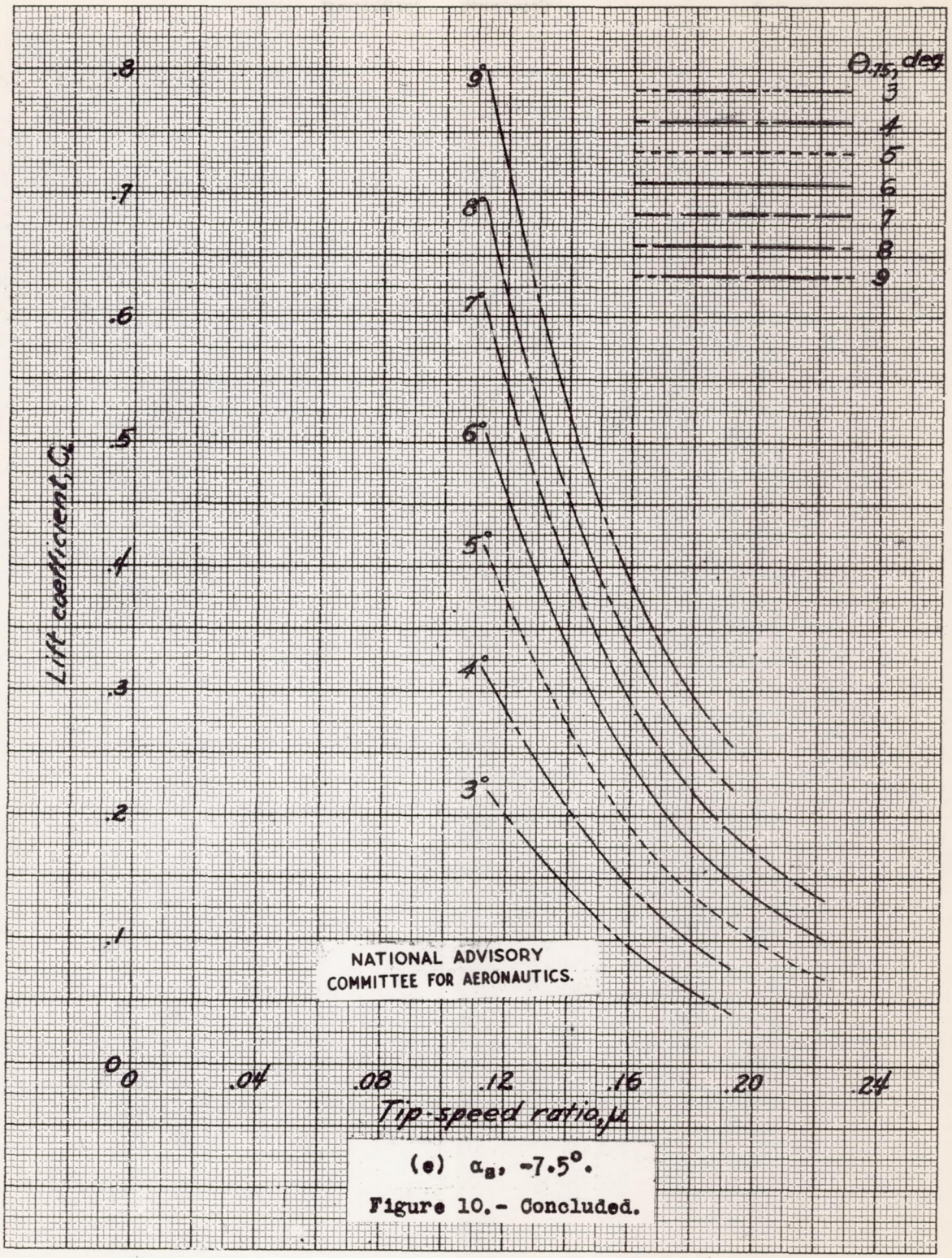

(e) α_s, -7.5°.

Figure 10.- Concluded.

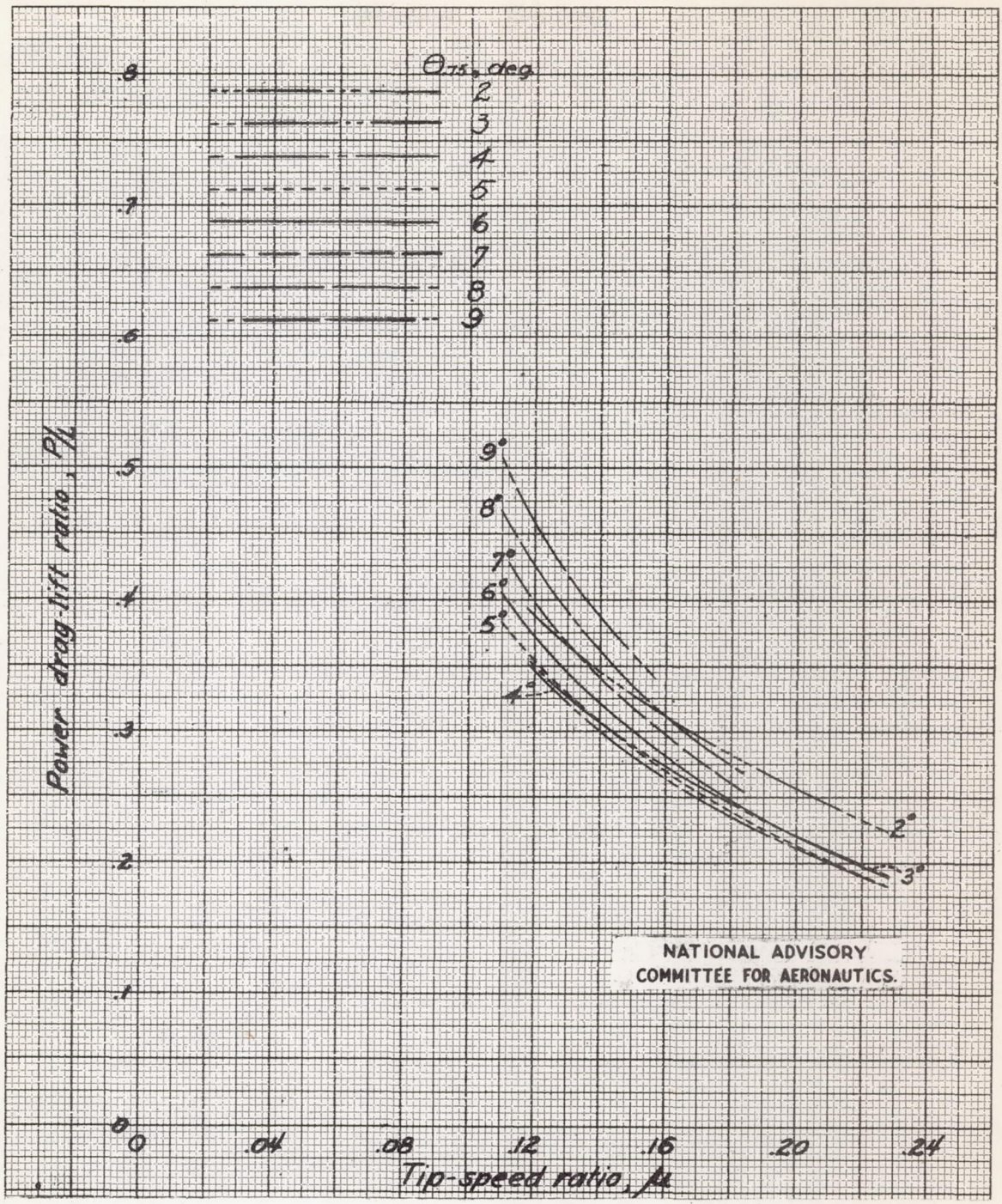

(a) α_s, -0.5°.

Figure 11.- Variation of power drag-lift ratio with tip-speed ratio for different values of pitch angle. PV-2 helicopter rotor; rotor speed, approximately 270 rpm.

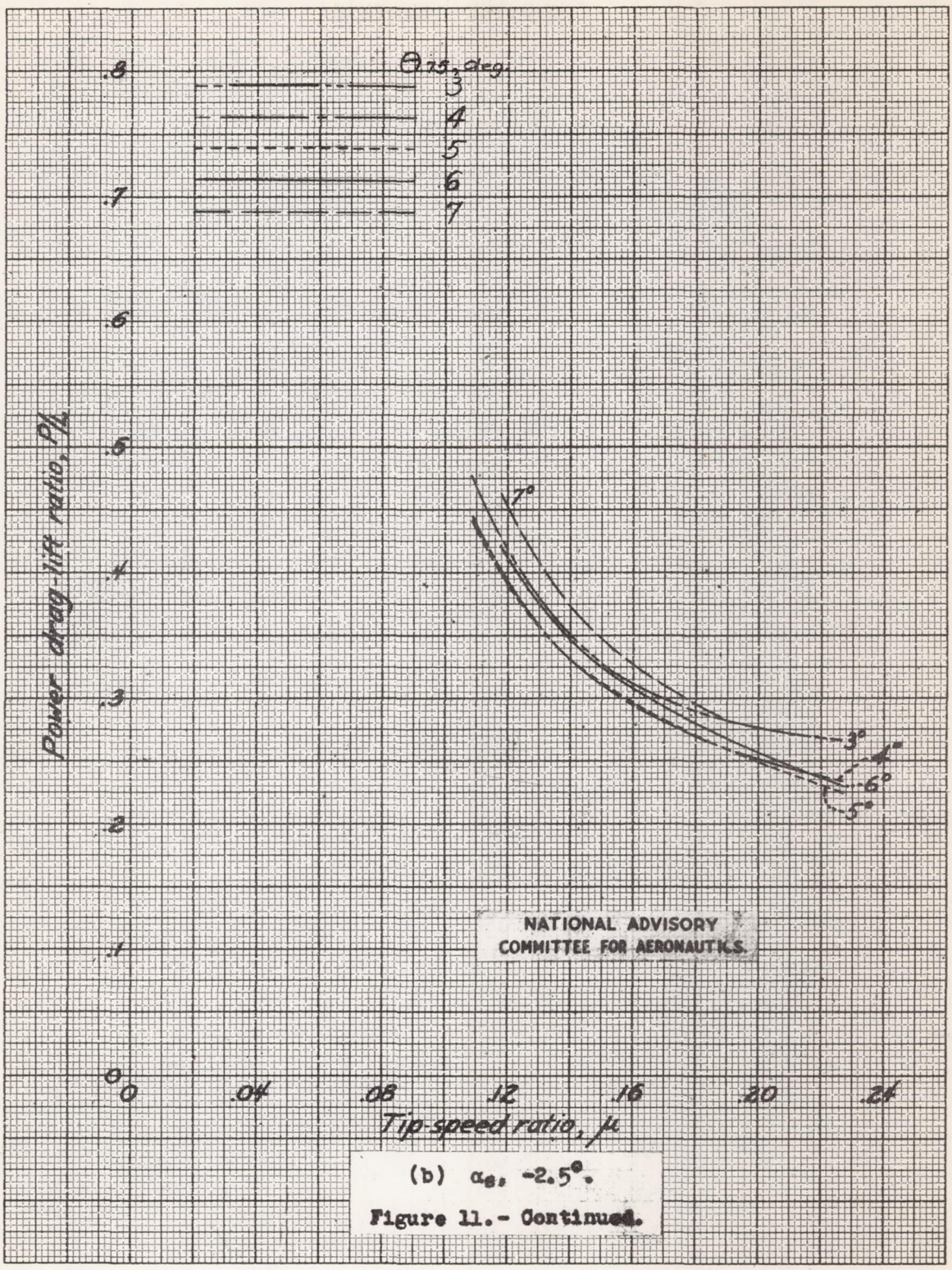

(b) α_s, -2.5°.

Figure 11.- Continued.

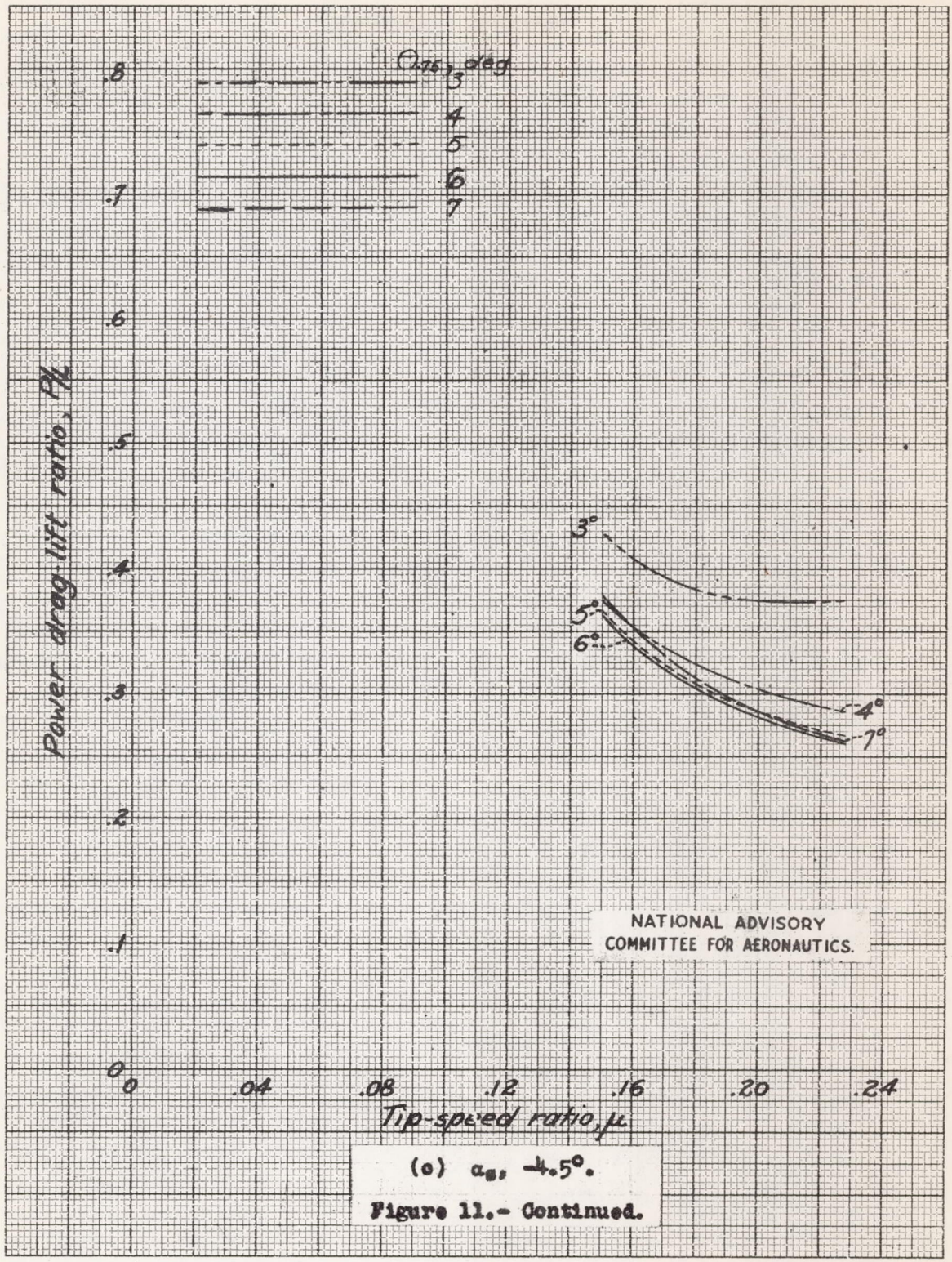

(c) α_s, -4.5°.

Figure 11.- Continued.

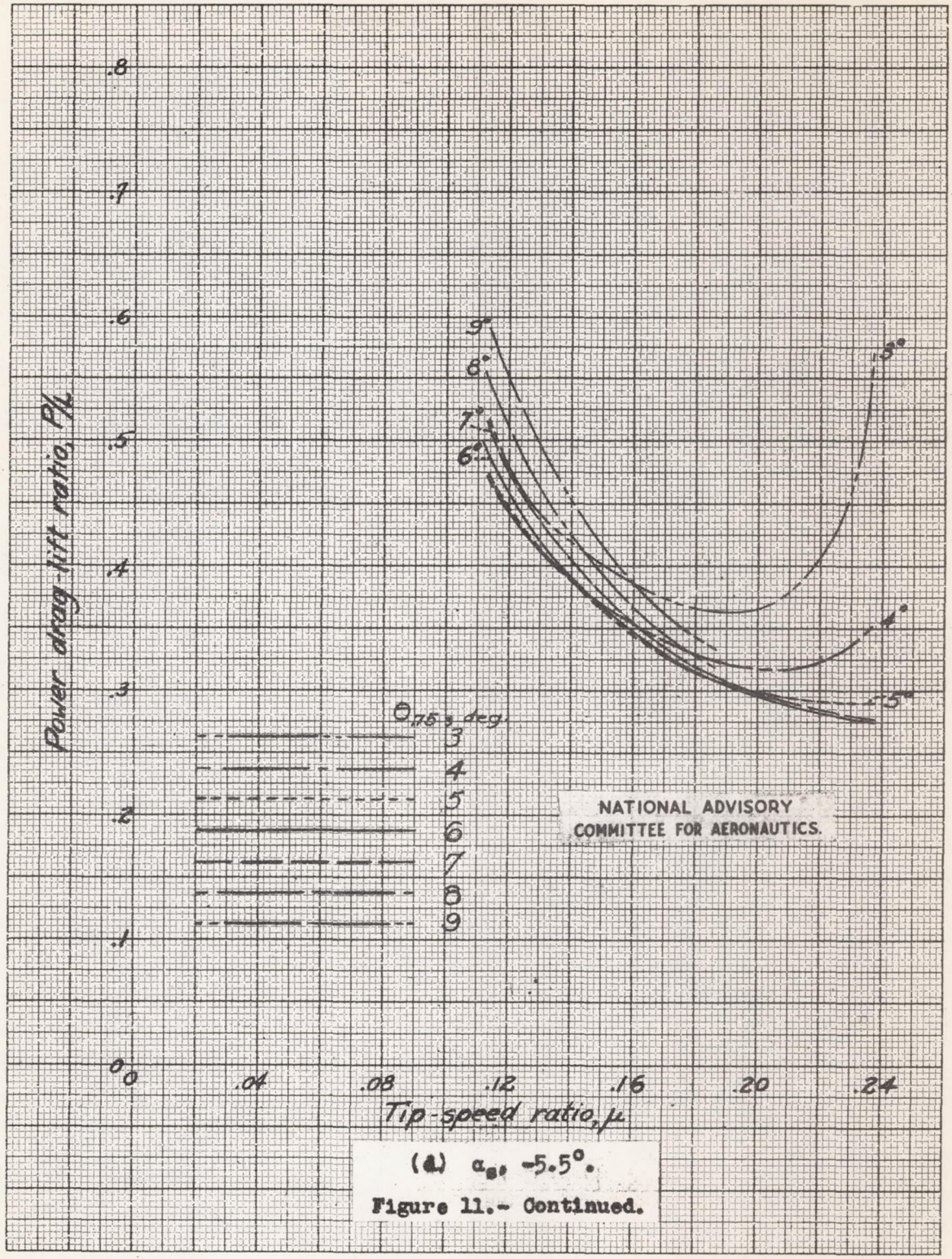

(d) α_s, -5.5°.

Figure 11.- Continued.

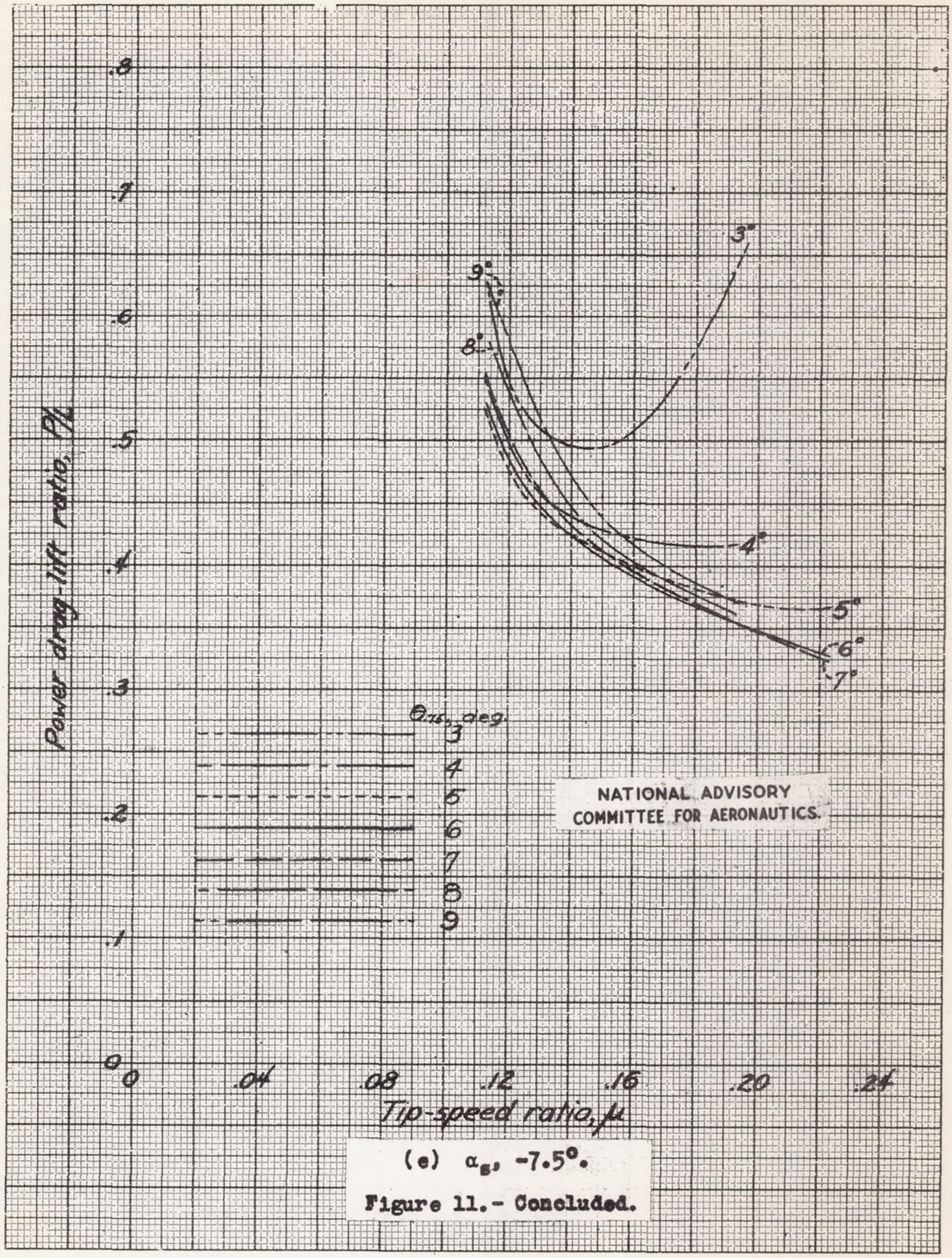

(e) α_s, -7.5°.

Figure 11.- Concluded.

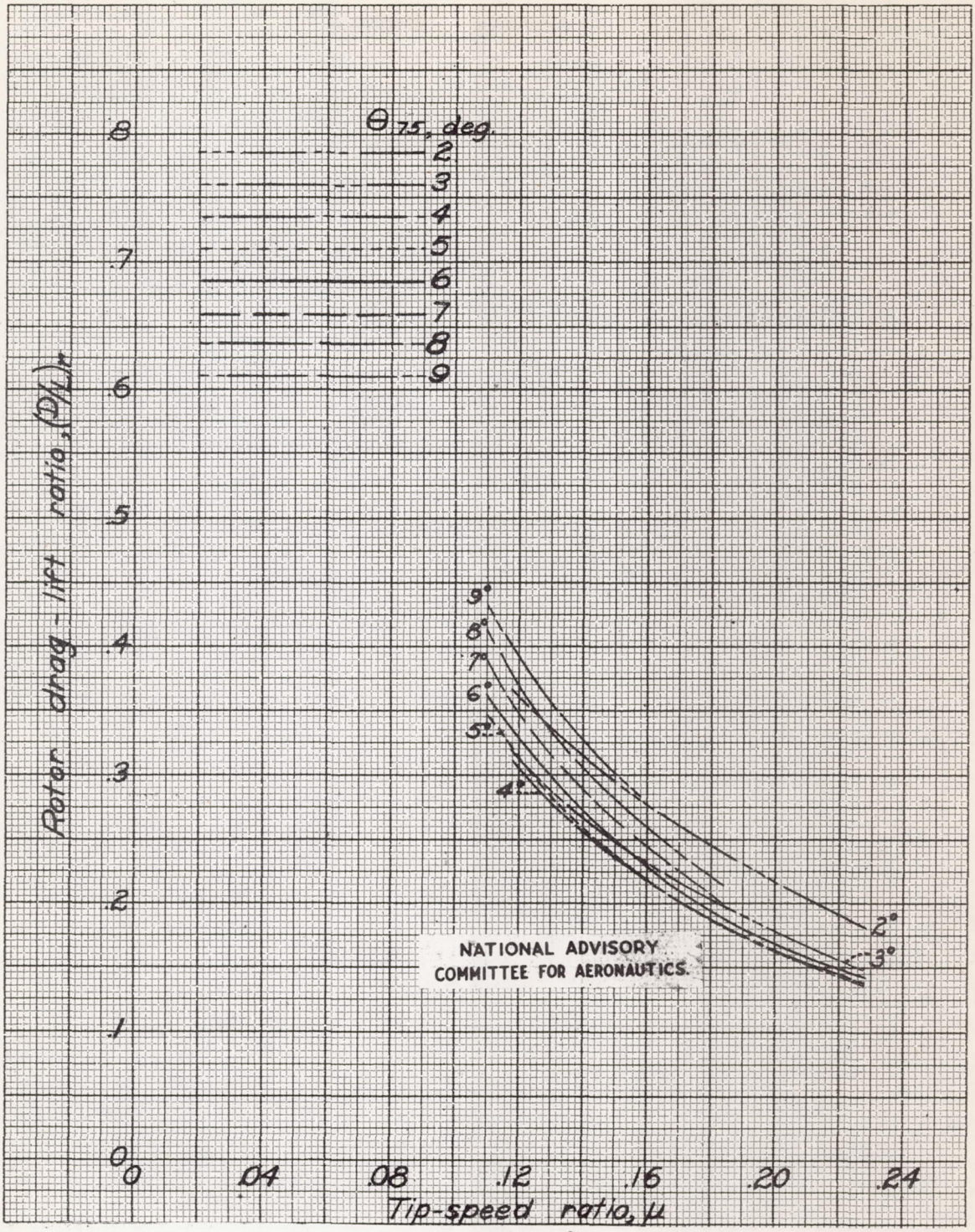

(a) α_s, -0.5°.

Figure 12.- Variation of rotor drag-lift ratio with tip-speed ratio for different values of pitch angle. PV-2 helicopter rotor; rotor speed, approximately 270 rpm.

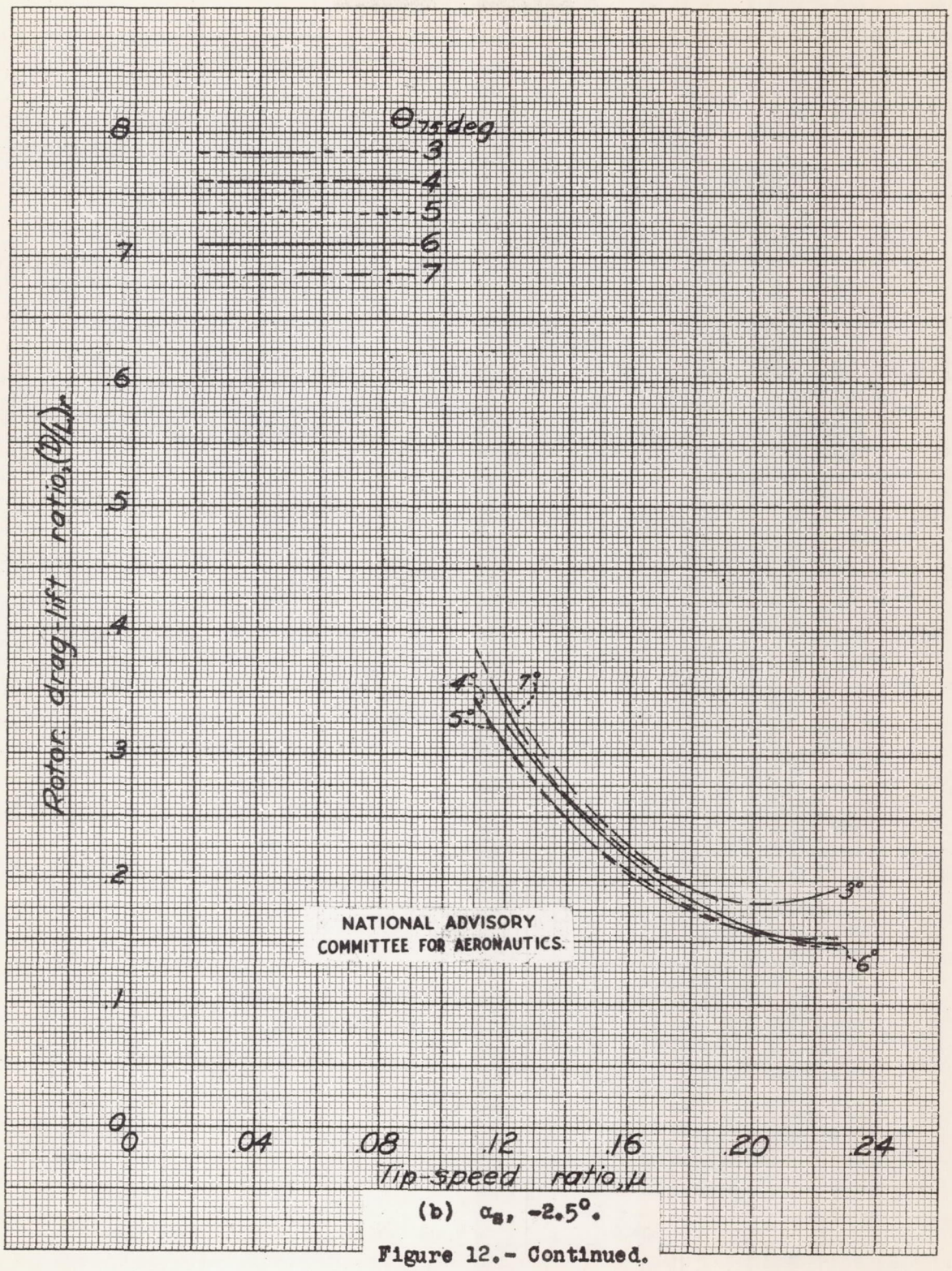

(b) α_s, -2.5°.

Figure 12.- Continued.

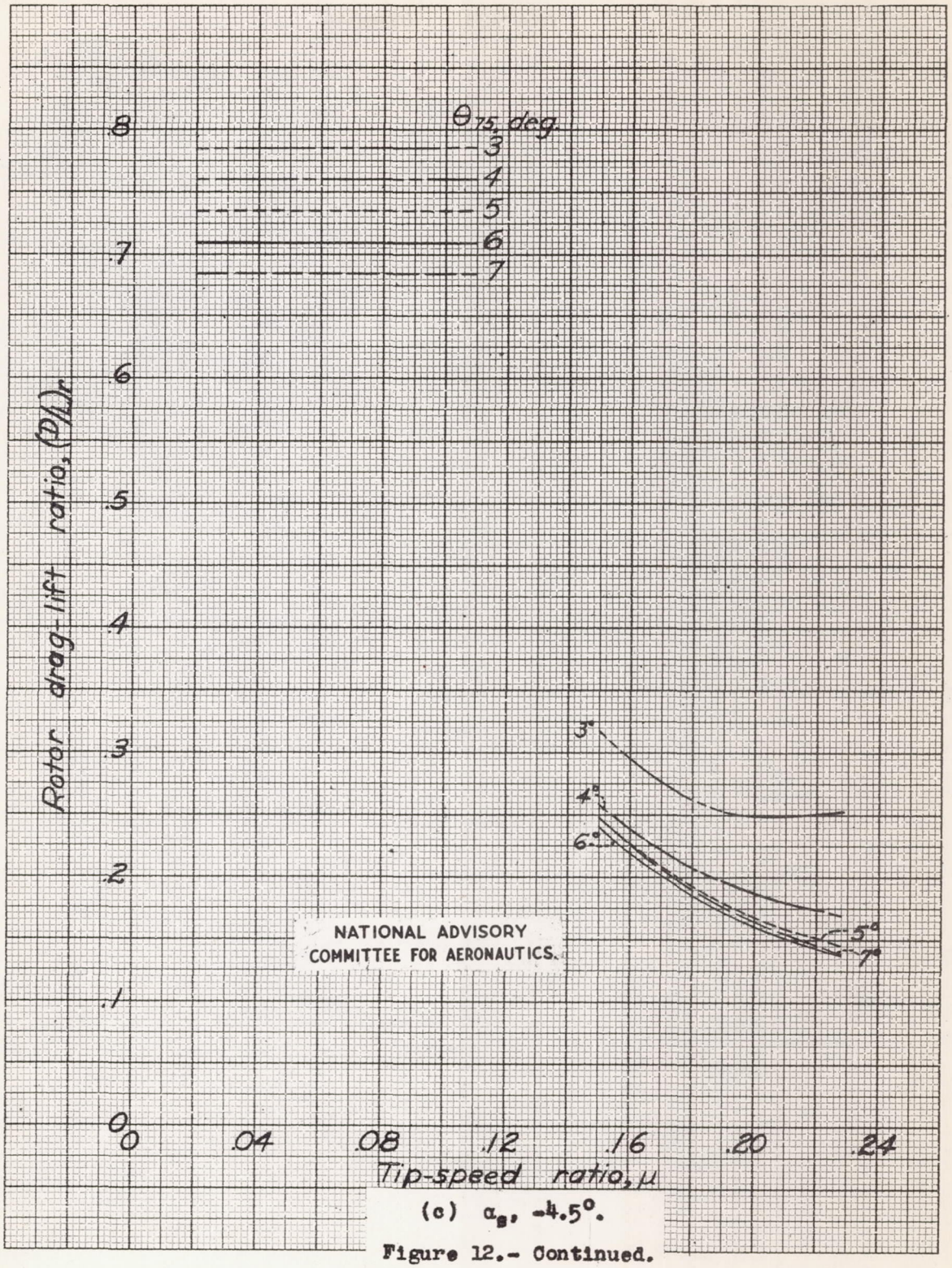

(c) α_s, -4.5°.

Figure 12.- Continued.

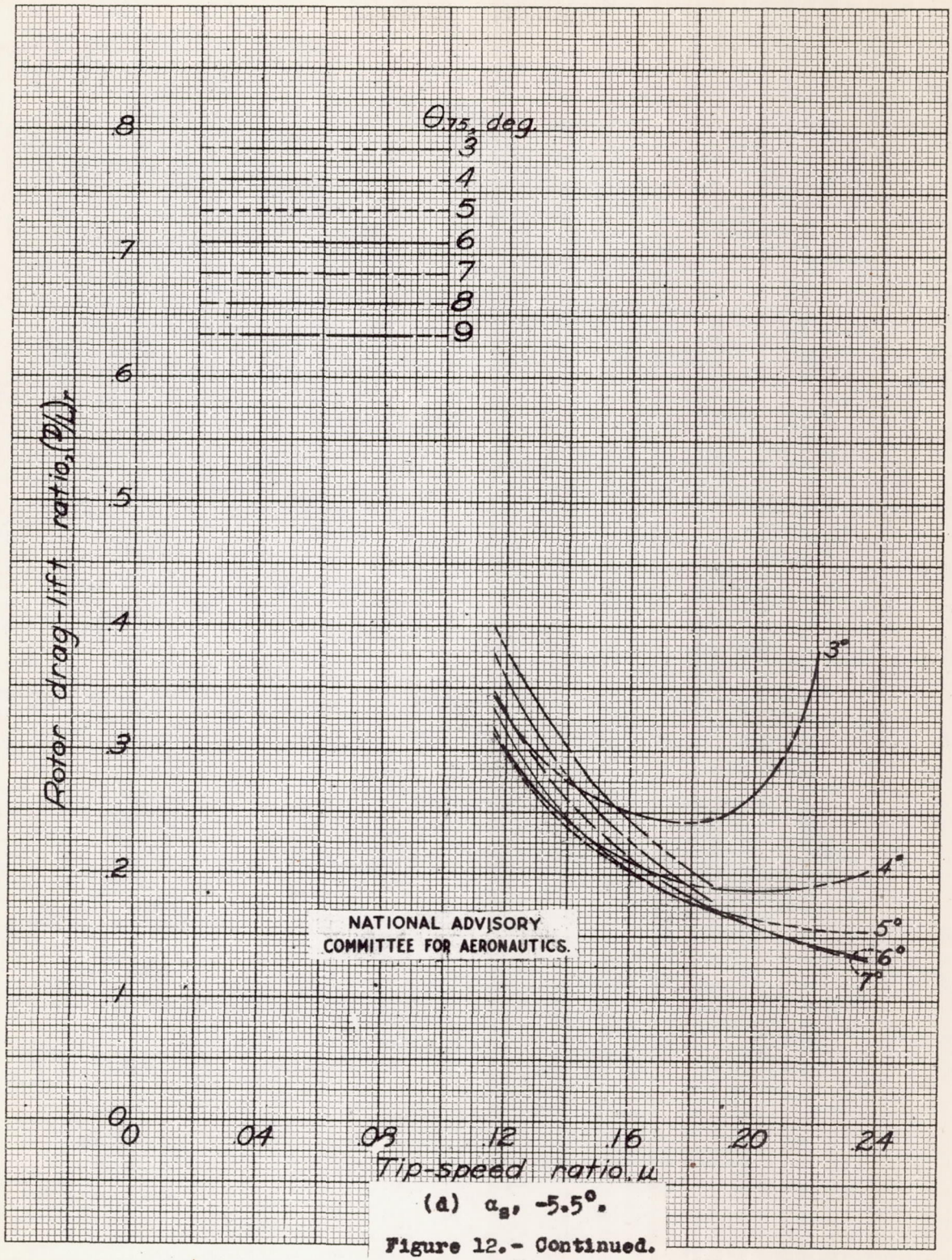

(a) α_s, -5.5°.

Figure 12.- Continued.

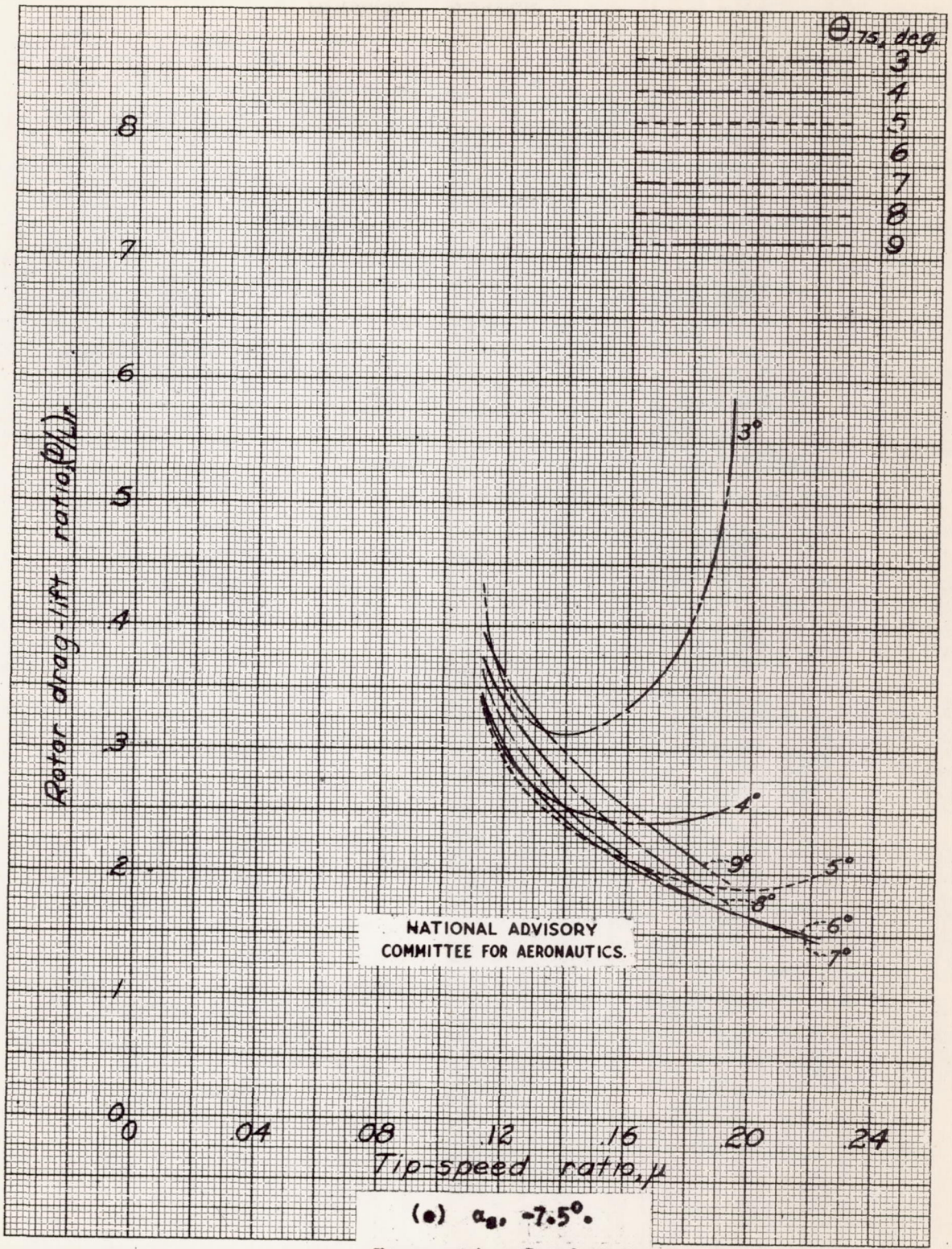

(e) α_s, -7.5°.

Figure 12.- Concluded.

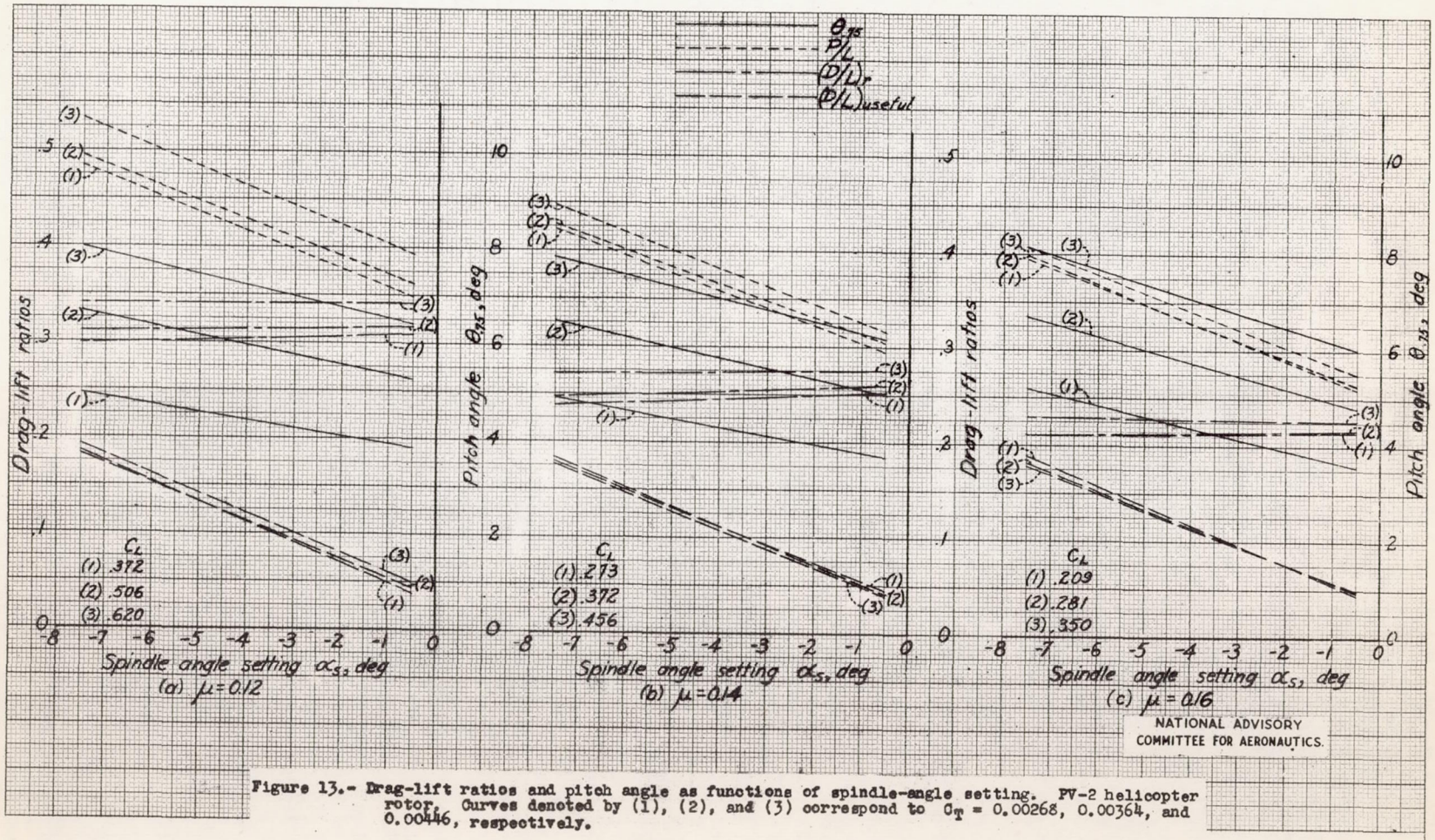

Figure 13.- Drag-lift ratios and pitch angle as functions of spindle-angle setting. PV-2 helicopter rotor. Curves denoted by (1), (2), and (3) correspond to C_T = 0.00268, 0.00364, and 0.00446, respectively.

MR No. L5C29a

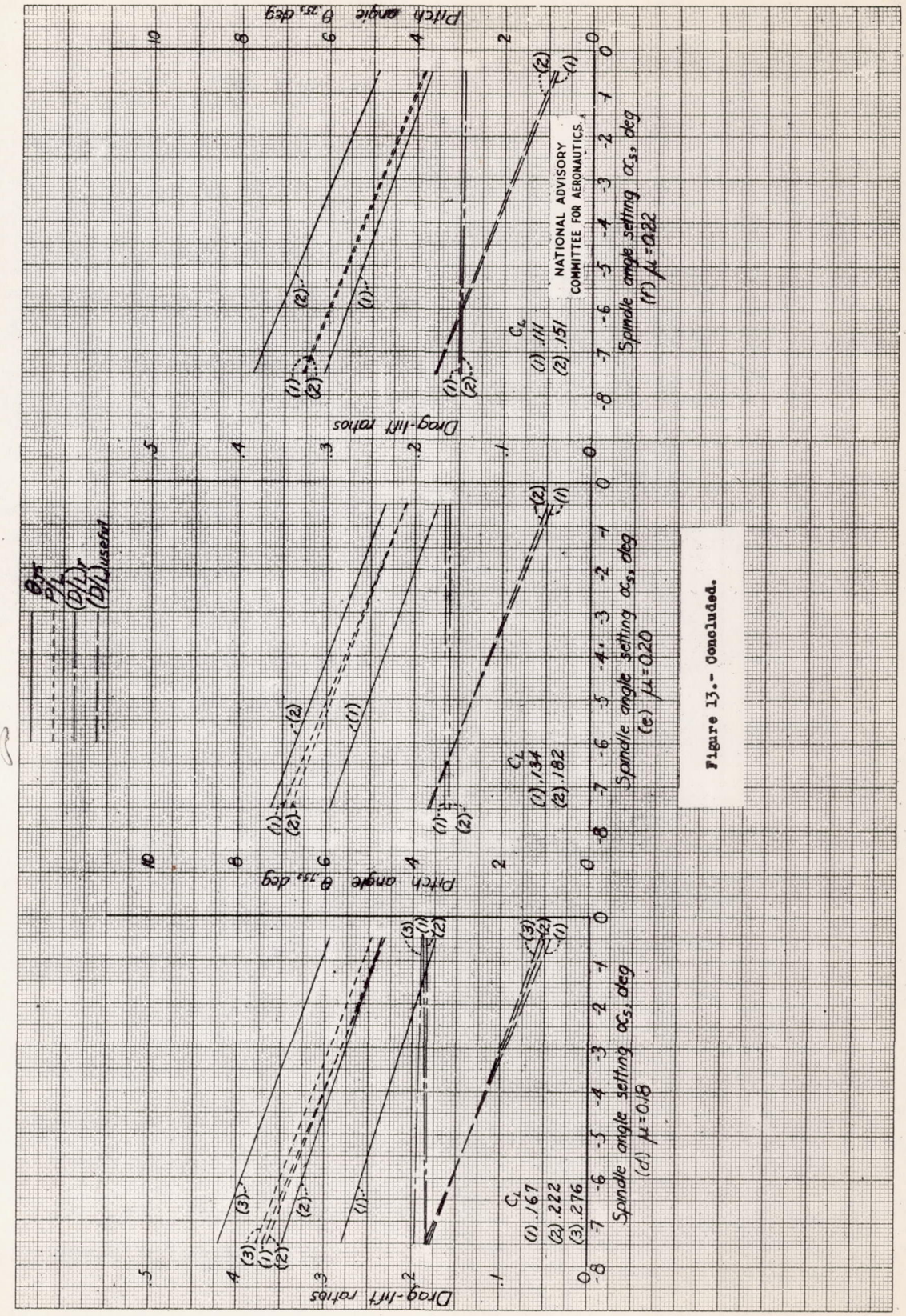

Figure 13.- Concluded.

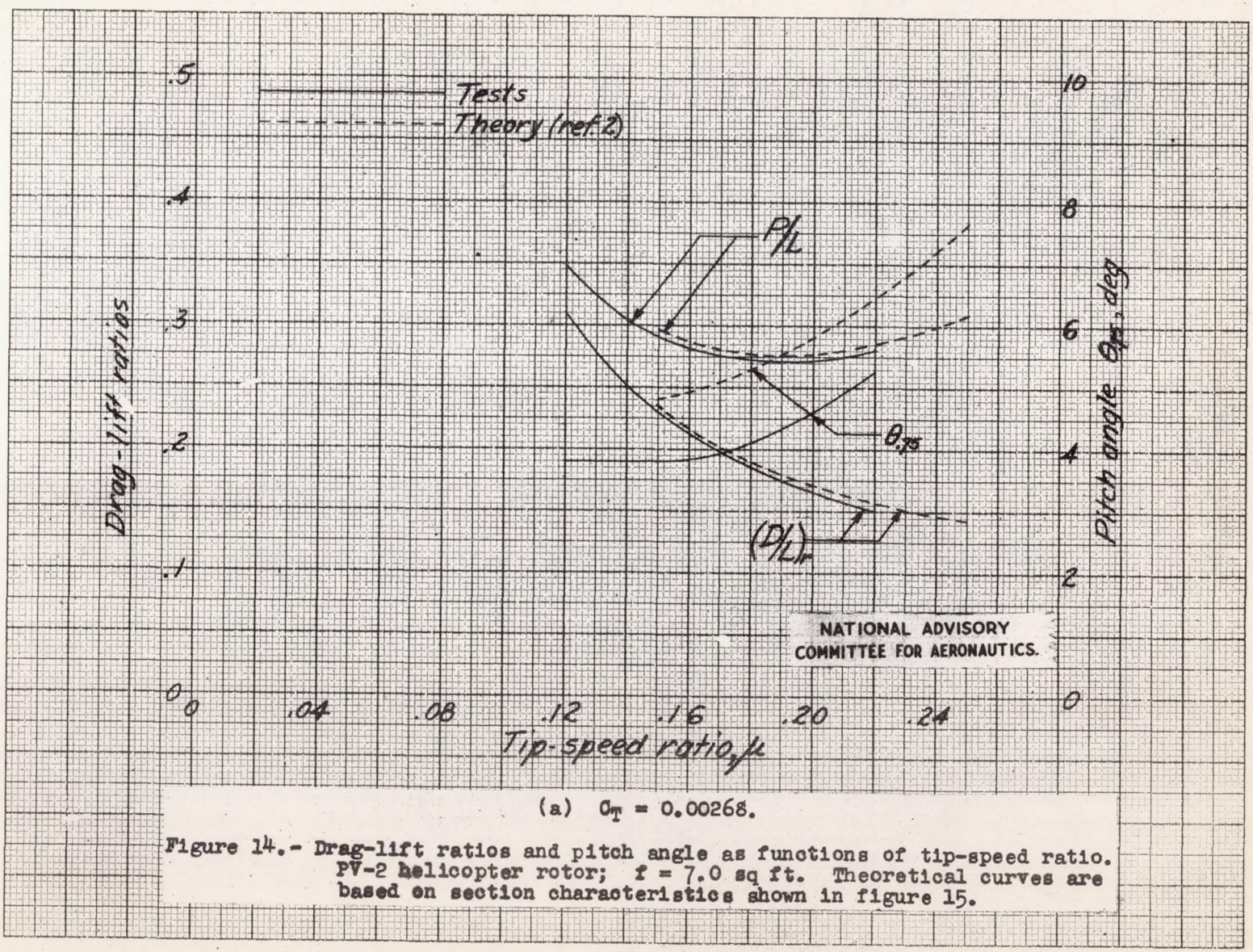

(a) $C_T = 0.00268$.

Figure 14.- Drag-lift ratios and pitch angle as functions of tip-speed ratio. PV-2 helicopter rotor; f = 7.0 sq ft. Theoretical curves are based on section characteristics shown in figure 15.

MR No. L5C29a

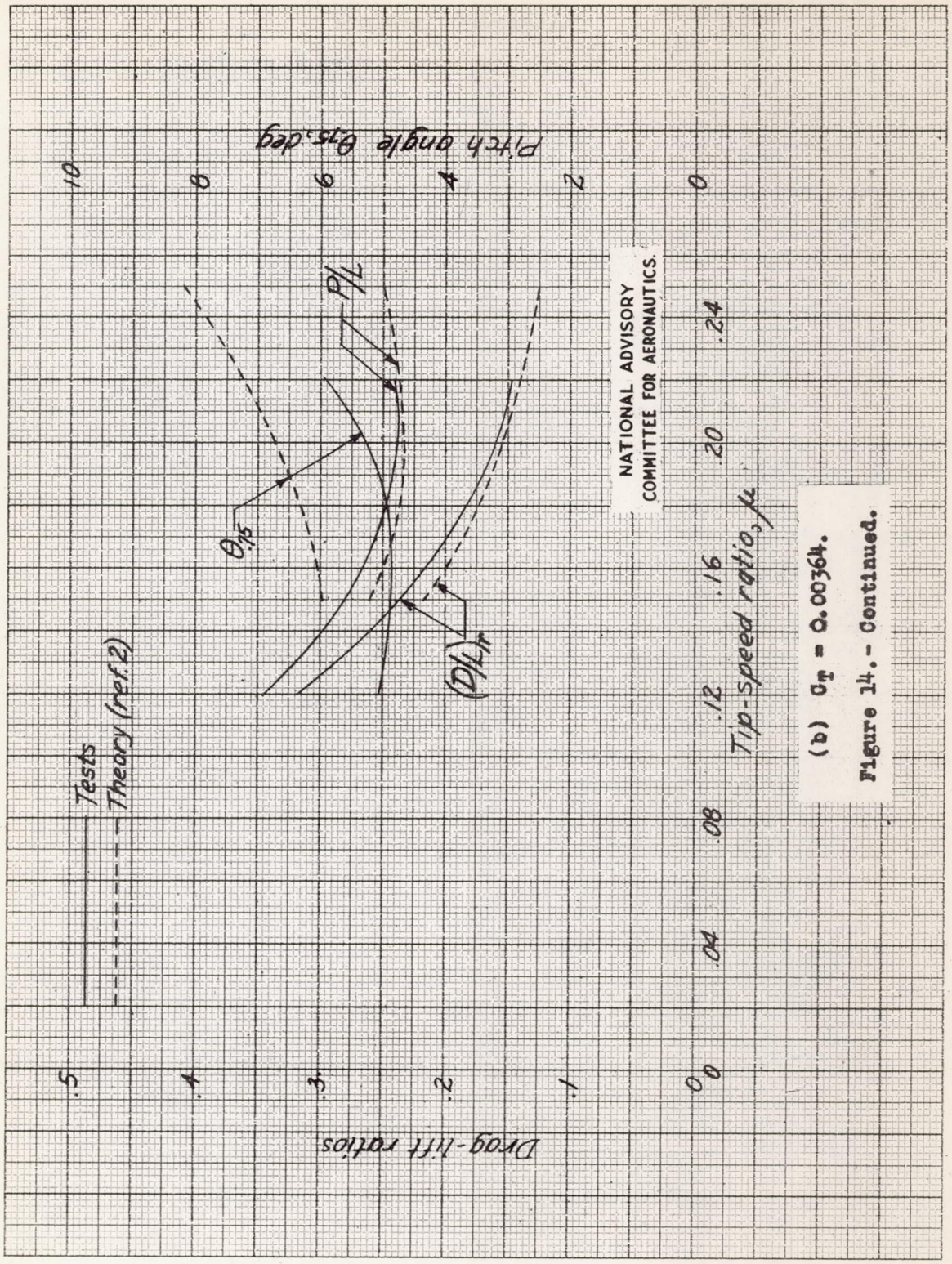

(b) $\sigma_r = 0.00364$.

Figure 14.- Continued.

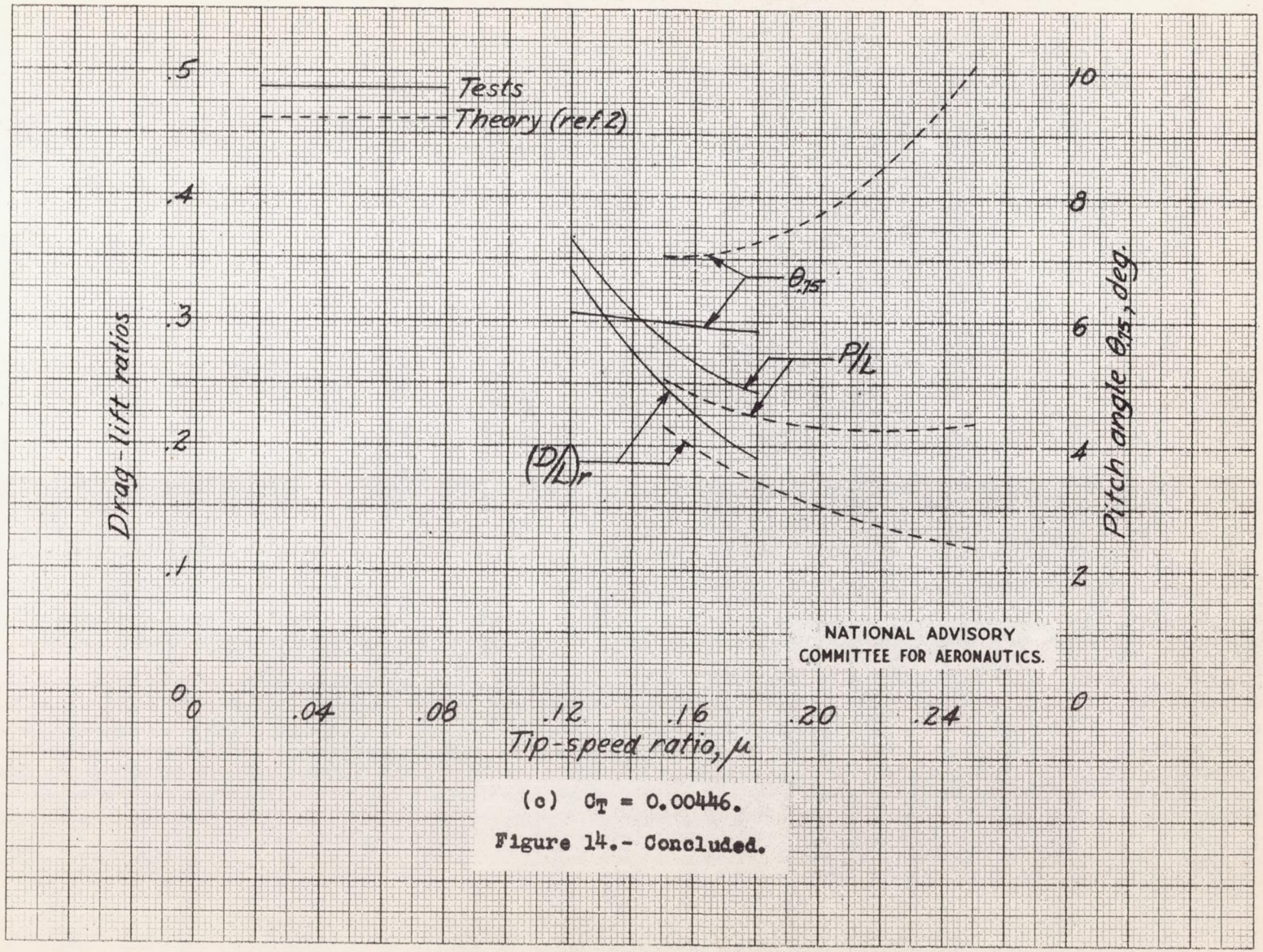

(c) $C_T = 0.00446$.

Figure 14.- Concluded.

MR No. L5C29a

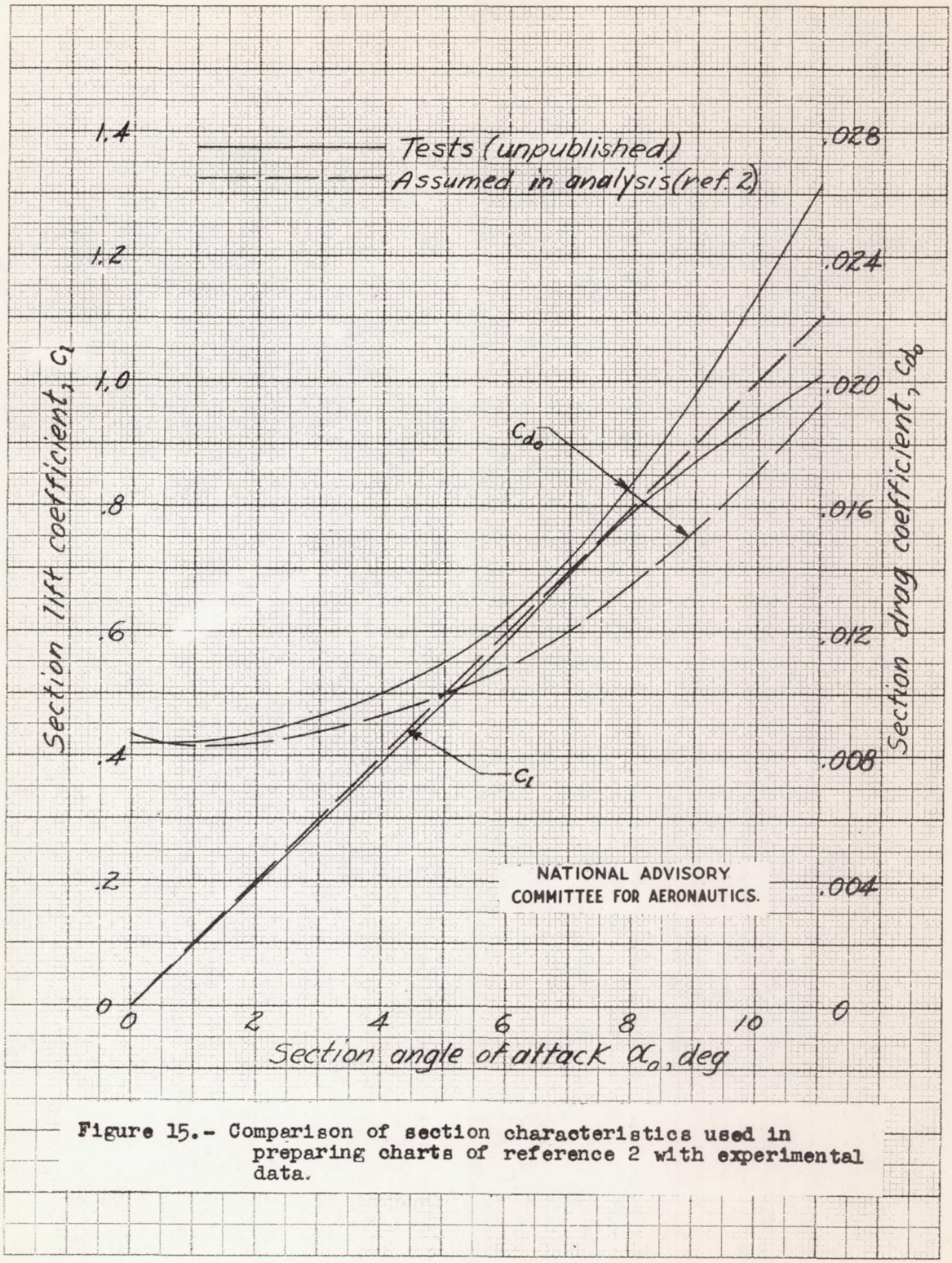

Figure 15.- Comparison of section characteristics used in preparing charts of reference 2 with experimental data.

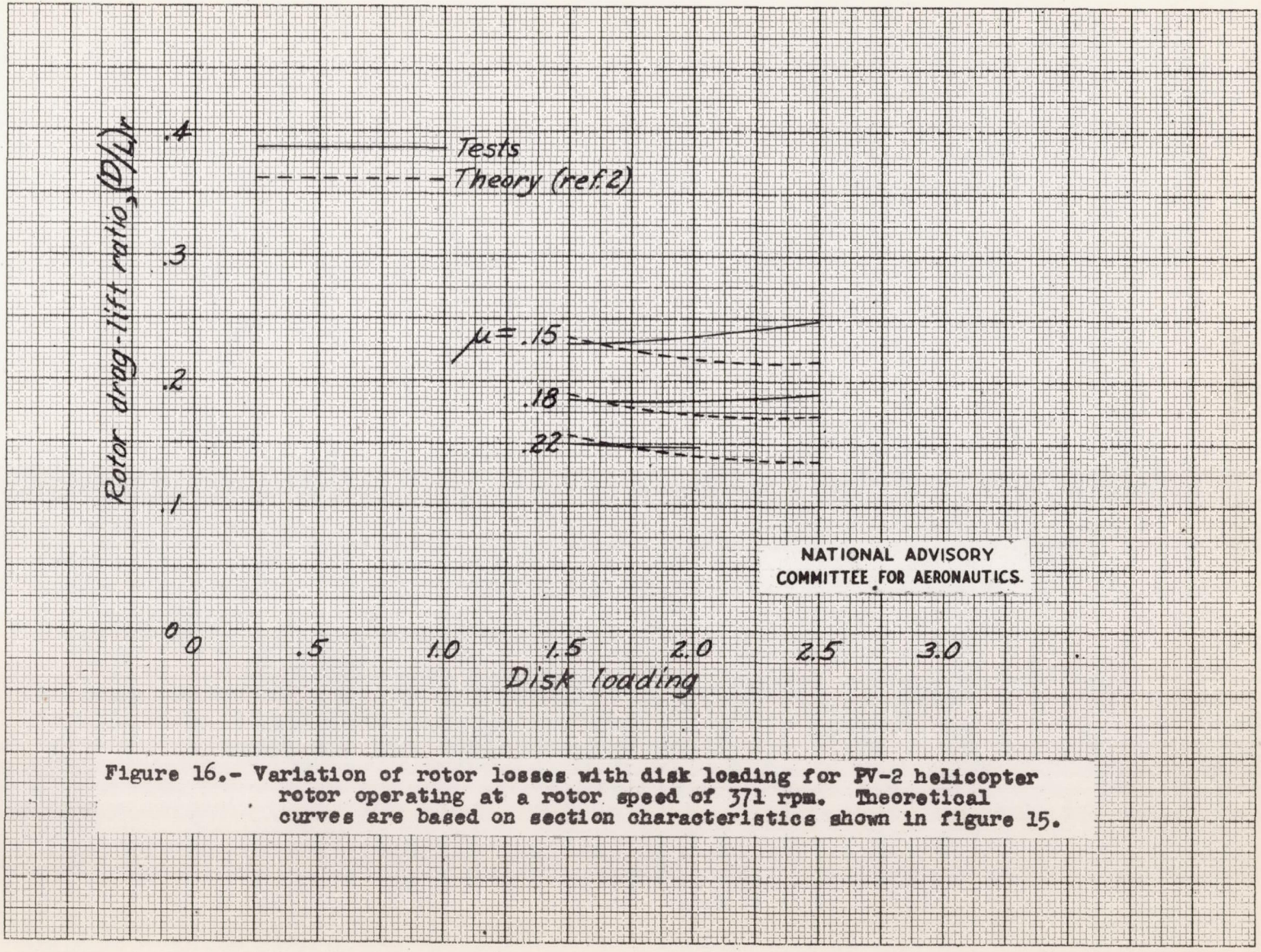

Figure 16.- Variation of rotor losses with disk loading for PV-2 helicopter rotor operating at a rotor speed of 371 rpm. Theoretical curves are based on section characteristics shown in figure 15.

MR No. L5C29a

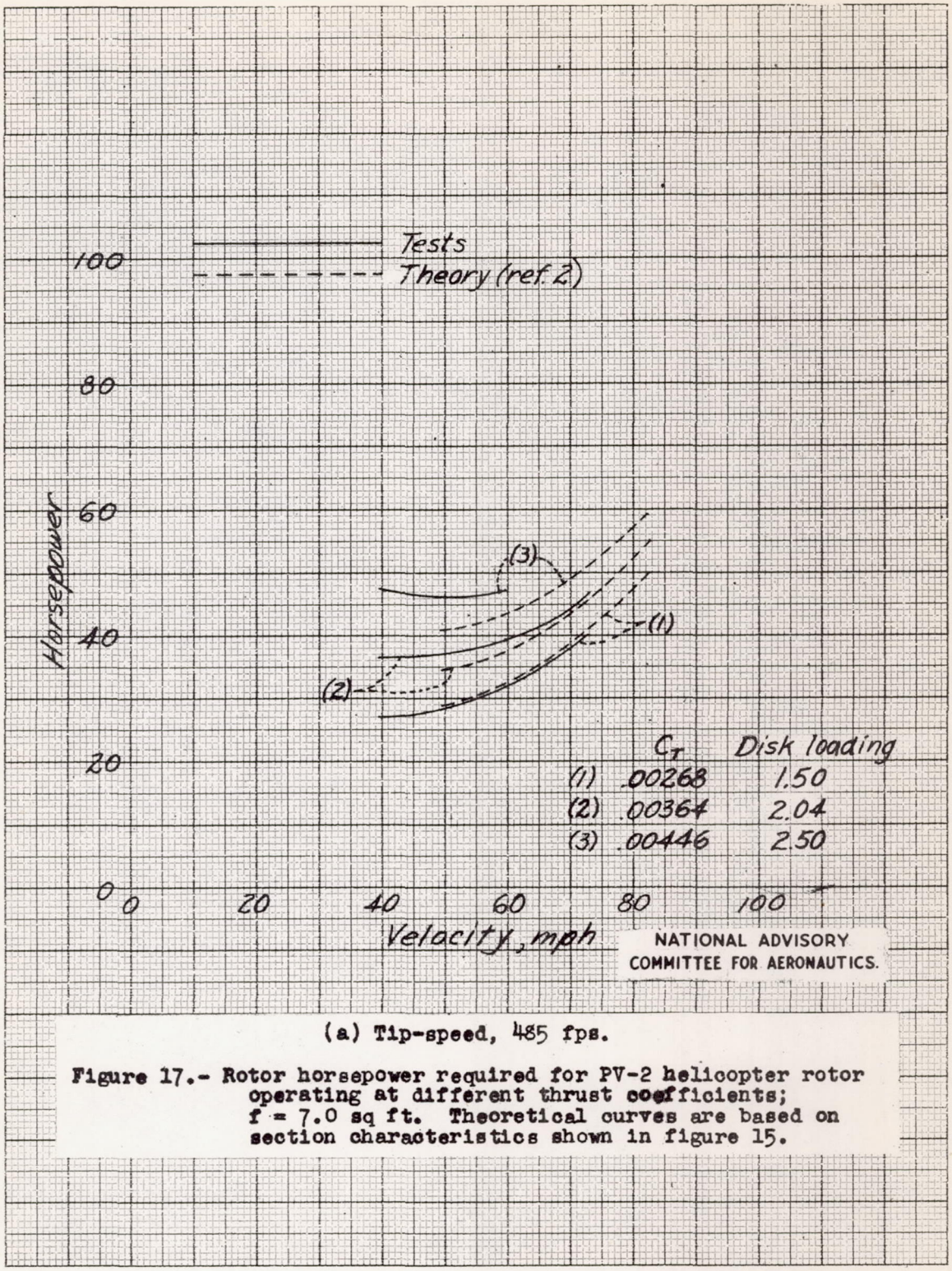

(a) Tip-speed, 485 fps.

Figure 17.- Rotor horsepower required for PV-2 helicopter rotor operating at different thrust coefficients; f = 7.0 sq ft. Theoretical curves are based on section characteristics shown in figure 15.

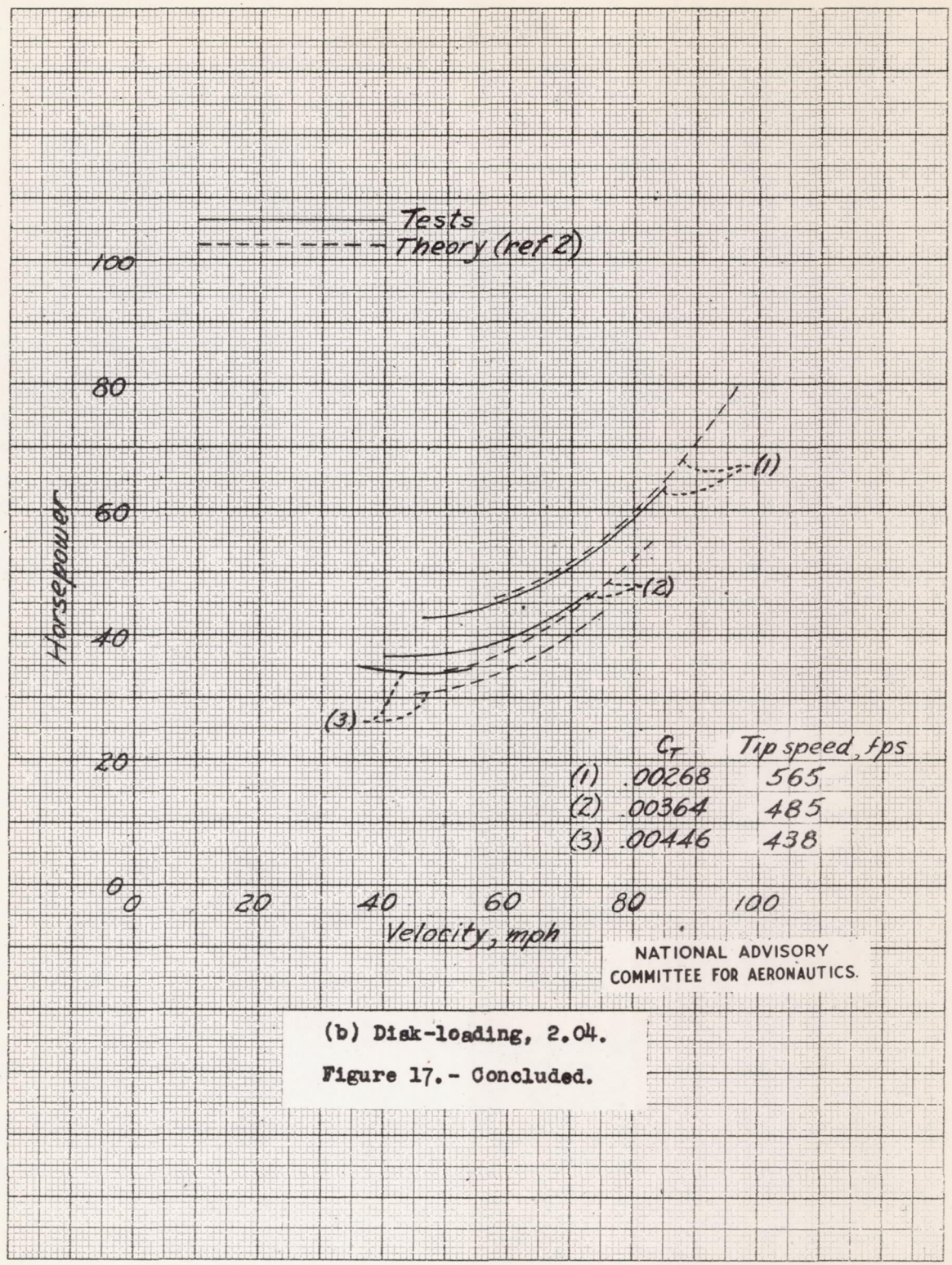

(b) Disk-loading, 2.04.

Figure 17.- Concluded.